AMERICAN JOURNAL OF PHYSIOLOGY
GASTROINTESTINAL AND LIVER PHYSIOLOGY

Am J Physiol Gastrointest Liver Physiol 328: G51–G71, 2025.
First published October 15, 2024; doi:10.1152/ajpgi.00110.2024

RESEARCH ARTICLE

Characterization of six clinical drugs and dietary intervention in the nonobese CDAA-HFD mouse model of MASH and progressive fibrosis

Malte Hasle Nielsen,[1] Jacob Nøhr-Meldgaard,[1] Mathias Bonde Møllerhøj,[1] Denise Oró,[1] Susanne E. Pors,[1] Maja Worm Andersen,[1] Ioannis Kamzolas,[2,3] Evangelia Petsalaki,[3] Michele Vacca,[2,4,5] Lea Mørch Harder,[6] James W. Perfield,[7] Sanne Veidal,[6] Henrik H. Hansen,[1] and Michael Feigh[1]

[1]Gubra, Hørsholm, Denmark; [2]TVP Lab, WT/MRC Institute of Metabolic Science, University of Cambridge, Cambridge, United Kingdom; [3]European Molecular Biology Laboratory, European Bioinformatics Institute (EMBL-EBI), Hinxton, United Kingdom; [4]Interdisciplinary Department of Medicine, University of Bari "Aldo Moro", Bari, Italy; [5]Laboratory of Liver Metabolism and MASLD, Roger Williams Institute of Hepatology, London, United Kingdom; [6]Research and Early Development, Novo Nordisk A/S, Måløv, Denmark; and [7]Lilly Research Laboratories, Eli Lilly and Company, Indianapolis, Indiana, United States

Abstract

The choline-deficient L-amino acid defined-high-fat diet (CDAA-HFD) mouse model is widely used in preclinical metabolic dysfunction-associated steatohepatitis (MASH) research. To validate the CDAA-HFD mouse, we evaluated disease progression and responsiveness to dietary and pharmacological interventions with semaglutide, lanifibranor, elafibranor, obeticholic acid (OCA), firsocostat, and resmetirom. Disease phenotyping was performed in C57BL/6J mice fed CDAA-HFD for 3–20 wk and ranked using the MASLD Human Proximity Score (MHPS). Semaglutide, lanifibranor, elafibranor, OCA, firsocostat, or resmetirom were profiled as treatment intervention for 8 wk, starting after 6 wk of CDAA-HFD feeding. Semaglutide and lanifibranor were further evaluated as early (preventive) therapy for 9 wk, starting 3 wk after CDAA-HFD diet feeding. In addition, benefits of dietary intervention (chow reversal) for 8 wk were characterized following 6 wk of CDAA-HFD feeding. CDAA-HFD mice demonstrated a nonobese phenotype with fast onset and progression of MASH and fibrosis, high similarity to human MASH-fibrosis, and tumor development after 20 wk of diet-induction. Semaglutide and lanifibranor partially reversed fibrosis when administered as prevention but not as treatment intervention. Elafibranor was the only interventional drug therapy to improve fibrosis. In comparison, chow-reversal resulted in complete regression of steatosis with improved liver inflammation and fibrosis in CDAA-HFD mice. CDAA-HFD mice recapitulate histological hallmarks of advanced MASH with progressive severe fibrosis, however, in the absence of a clinical translational obese dysmetabolic phenotype. CDAA-HFD mice are suitable for profiling drug candidates directly targeting hepatic lipid metabolism, inflammation, and fibrosis. The timing of pharmacological intervention is critical for determining antifibrotic drug efficacy in the model.

NEW & NOTEWORTHY The CDAA-HFD mouse model is widely used in preclinical MASH research, but validation of the model is lacking. This study presents the longitudinal characterization of disease progression. Furthermore, late-stage clinical compounds and dietary intervention (chow reversal) display distinct hepatoprotective effects in the model. Collectively, the study provides critical information guiding the use of the CDAA-HFD mouse model in preclinical drug discovery for MASH and fibrosis.

CDAA-HFD mouse; metabolic dysfunction-associated steatohepatitis; fibrosis; disease progression; treatment intervention

INTRODUCTION

Metabolic dysfunction-associated steatotic liver disease [MASLD, formerly known as nonalcoholic fatty liver disease (NAFLD)] encompasses a spectrum of liver conditions, ranging from simple steatosis to metabolic dysfunction associated steatohepatitis [MASH, formerly known as nonalcoholic steatohepatitis (NASH)]. MASH is characterized by hepatocyte injury (hepatocyte ballooning) and inflammation carrying an increased risk of liver fibrosis, which is the strongest predictor of disease progression and mortality in MASLD (1). MASH can develop asymptomatically over decades and may progress to cirrhosis, hepatocellular carcinoma (HCC), and ultimately liver failure and premature death. The global prevalence of MASLD is estimated to have passed 30%, driven by the epidemics of obesity and type 2 diabetes, thus being a significant burden on global public health (2). Treatment options are limited for MASH, comprising dietary and lifestyle intervention. As a landmark in clinical drug development for MASH, FDA has recently granted accelerated approval for resmetirom (Rezdiffra), a liver-targeted thyroid hormone receptor β (THR-β) agonist, in conjunction with diet and exercise for the treatment of patients with MASH with moderate to advanced liver fibrosis (3, 4). Considering

Correspondence: M. H. Nielsen (mni@gubra.dk).
Submitted 10 April 2024 / Revised 13 September 2024 / Accepted 23 September 2024

the relatively moderate response rate and efficacy of resmetirom (5), there will be a continuous need for drugs with improved efficacy profiles for more effective management of MASH.

The complex molecular signaling mechanisms involved in the onset and progression of MASH are reflected in the diverse range of drug targets currently pursued in preclinical and clinical drug discovery (6, 7). Nutrient-deficient models, based on diets that are low or devoid of the essential amino acids methionine and/or choline, are widely used in preclinical drug discovery. Dietary deficiency of the lipotropic amino acid choline impedes phospholipid synthesis thereby impairing very-low-density lipoprotein (VLDL) packaging, reducing hepatic fatty acid oxidation and export of triglycerides. This results in increased intrahepatic oxidative stress and excessive lipid accumulation, which triggers rapid onset of liver inflammation and fibrosis, however, in the context of halted growth (8, 9). One of the most common nutrient-deficient models used in preclinical drug discovery is based on feeding with a choline-deficient L-amino acid-defined (CDAA) diet, where choline has been substituted with an equivalent mixture of L-amino acids (10). CDAA diet feeding promotes the rapid onset of MASH and the development of fibrosis within 6 wk (11). Further extension of the CDAA feeding period causes manifest cirrhosis and development of hepatocellular carcinoma (HCC) (12, 13). High-fat diet (HFD) and sugar supplementation have been introduced to prevent marked CDAA diet-induced weight loss (11, 13, 14). In addition, cholesterol supplementation can further accelerate disease progression in CDAA diet-fed rodents (15). The rapid development of histological features of MASH with severe fibrosis in CDAA-HFD mice makes the model attractive for screening of potential antifibrotic drug candidates. Despite the wide use in preclinical research, few studies have longitudinally characterized disease progression in CDAA-HFD mice (11, 16) and head-to-head efficacy studies on clinically relevant compounds are lacking in the model.

To further validate the CDAA-HFD mouse as an applicable model in preclinical drug discovery, the current study aimed to profile disease progression in the model and compare treatment interventional effects of six compounds evaluated in phase-2/3 trials for MASH. These included semaglutide (long-acting glucagon-like peptide-1 receptor 1 (GLP-1R) agonist) (17); lanifibranor [peroxisome proliferator-activated receptor (PPAR)-α/δ/λ agonist] (18); elafibranor (PPAR-α/δ agonist) (19); obeticholic acid [OCA, farnesoid X receptor (FXR) agonist] (20); firsocostat [acetyl-CoA carboxylase (ACC) inhibitor] (21), and resmetirom [thyroid hormone receptor β (THR-β) agonist] (5). The efficacy of drug therapies was compared with dietary intervention (chow-reversal). The CDAA-HFD mouse model was also characterized in the context of early-stage disease management, i.e., before the onset of liver fibrosis, by early introduction (preventive therapy) of semaglutide and lanifibranor monotherapy.

MATERIALS AND METHODS

Ethics

All animal experiments were approved by the Danish Animal Experiments Inspectorate and adhered to internationally accepted principles for the use of laboratory animals (license no. 2013-15-2934-00784). Animal experiments were conducted in accordance with Gubra bioethical guidelines, which are fully compliant with internationally accepted principles for the care and use of laboratory animals.

Animals

Male C57BL/6J mice were purchased from Janvier Labs (Le Genest Saint Isle, France) at 9 to 10 wk of age and housed in a controlled environment (12-h light/dark cycle, lights on at 3:00 AM, 21 ± 2°C, humidity 50 ± 10%). Animals were identified by an implantable subcutaneous microchip (PetID Microchip, E-vet, Haderslev, Denmark). Mice had ad libitum access to tap water and chow (3.22 kcal/g, Altromin 1324, Brogaarden, Hørsholm, Denmark) or a choline-deficient L-amino acid-defined, high-fat diet [CDAA-HFD; 45 kcal-% fat with 0.1% methionine, no added choline, 1% cholesterol, 28 kcal-% fructose, A16092201, Research Diets, New Brunswick, NJ (see Supplemental Table S1 for full nutrient composition)] for 3, 6, 12, or 20 wk ($n = 12$ per time point; see study outline in Fig. 2*A*). Mice fed with chow for 8–20 wk (total 8–12/time-point, total $n = 26$), served as healthy controls. Animals were terminated by cardiac puncture under isoflurane anesthesia (Vetflurane, Virbac, Kolding, Denmark).

Dietary Intervention

For the chow reversal study, mice were randomized according to body weight determined 3 days before the study start. A baseline group was terminated at the study start, after the completion of 6 wk of CDAA-HFD diet induction. At study start, CDAA-HFD fed mice were switched to chow or remained on CDAA-HFD for 8 wk ($n = 12$ per group) (Fig. 5*A*). Mice fed chow throughout served as healthy controls ($n = 8$). Body weight was measured daily throughout the in vivo phase.

Pharmacological Intervention

Treatment with semaglutide, elafibranor, OCA, firsocostat, lanifibranor, and resmetirom was characterized in CDAA-HFD mice in the context of treatment intervention. Lanifibranor was further characterized in the context of preventive therapy, i.e., initiation of treatment before the onset of fibrosis. Animals were randomized and stratified to treatment according to body weight determined three days before study start. Baseline groups were terminated after completion of the corresponding CDAA-HFD diet induction period. Prevention therapy was initiated after 3 wk of CDAA-HFD feeding (Fig. 7*A*), whereas treatment intervention was started after 6 wk of CDAA-HFD feeding (Fig. 6*A*). CDAA-HFD mice ($n = 10$–12 per group) were administered vehicle, semaglutide (30 nmol/kg sc, daily), elafibranor (30 mg/kg po, daily), OCA (30 mg/kg, po, daily), firsocostat (5 mg/kg po, daily), lanifibranor (30 mg/kg po, daily), or resmetirom (1 mg/kg po, daily) for 8 wk. In the setting of prevention therapy, semaglutide and lanifibranor were administered for 9 wk. Mice remained on the CDAA-HFD throughout the study. Vehicles and compounds were administered in a dosing volume of 5 mL/kg. Body weight was measured daily throughout the in vivo phase.

Glucose Tolerance Test

An intraperitoneal glucose tolerance test (ipGTT) was performed in mice fed chow or CDAA-HFD for 10 wk. Animals were fasted for 4 h after which an intraperitoneal glucose bolus (2 g glucose/kg, 10 mL/kg; Fresenius Kabi, Uppsala, Sweden) was administrated at $t = 0$. Blood samples were collected from the tail vein (20 μL per sample) at $t = 0$, 15, 30, 60, 120, and 180 min for measuring blood glucose. The glucose area under the curve (AUC, 0–180 min) was determined.

Plasma and Liver Biochemistry

Four-hour fasted terminal blood was sampled from the tail vein, kept on ice, and centrifuged (5 min, 4°C, 6,000 *g*) to generate EDTA-stabilized plasma assayed for insulin, alanine aminotransferase (ALT), aspartate aminotransferase (AST), triglycerides (TGs), total cholesterol (TC), and liver TG and TC, as described previously (22). For the determination of hydroxyproline (HP), quick-frozen liver tissue (100 mg) was homogenized in 6MHCl and hydrolyzed to degrade collagen. Hydroxyproline content was then measured in the supernatant using a colorimetric kit (Cat. No. QZBHYPRO5, Quickzyme Biosciences, Leiden, The Netherlands) according to the manufacturer's instructions. The HOMA-IR (homeostasis model assessment of insulin resistance) index was calculated using the standard equation [fasting plasma insulin (mU/L) × fasting blood glucose (mmol/L)/22.5], as previously described (23). Plasma markers of fibrosis included amino-terminal propeptide of type III procollagen (PIIINP, no. CSB-E08095m, CusaBio, Houston, TX) and tissue inhibitor of metalloproteinase-1 (TIMP-1). PIIINP was determined according to the manufacturer's instructions, TIMP-1 was assayed, as previously described (24).

Liver Histology

A terminal liver biopsy (≈200 mg) was dissected from the left lateral lobe, fixed overnight in 4% paraformaldehyde, paraffin-embedded, and sectioned (3 μm thickness). Sections were stained with hematoxylin-eosin (HE), picrosirius red (PSR; Sigma-Aldrich, Brøndby, Denmark), anti-galectin-3 (cat. 125402, Biolegend, San Diego, CA), anti-α-smooth muscle action (α-SMA, cat. Ab124964; Abcam, Cambridge, UK) or anti-type I collagen (Col1a1, cat. 1310-01, Southern Biotech, Birmingham, AL) using standard procedures (22, 25).

Automated Deep Learning-Based Image Analysis

Histopathological scoring of steatosis, lobular inflammation, hepatocyte ballooning, and fibrosis staging was performed by Gubra Histopathological Objective Scoring Technology (GHOST) automated deep learning-based image analysis (see later) according to the MASH CRN scoring system as outlined by Kleiner et al. (26). The deep learning-based image analysis tool has previously been described in detail by Møllerhøj et al. (27). For fibrosis staging, the image analysis tool was further trained with PSR-stained liver biopsies from CDAA-HFD mice for more accurate detection of central veins and portal triads. The bridging segmentation was also adjusted to CDAA-HFD liver samples. Deep learning-based image analysis was further applied for quantitative histology assessment of the fraction (%) of lipid-laden hepatocytes, number of inflammatory foci (foci/mm^2), and proportionate (%) area of periportal and sinusoidal fibrosis. Digital imaging software (Visiomorph, Visiopharm, Hørsholm, Denmark) was used for determining levels of liver fat (HE-staining), fibrosis (PSR, Col1a1), inflammation (galectin-3), and activation of hepatic stellate cells (HSCs) (α-SMA), expressed relative (%) to the total liver sectional area. To account for treatment-induced changes in liver mass, whole liver marker content (mg) was estimated by multiplying the percent area of positive staining with corresponding total liver weight, as described previously.

RNA Sequencing

Liver transcriptome analysis was performed by RNA sequencing on RNA extracts from terminal liver samples (15 mg fresh tissue), as described in detail elsewhere (24). RNA sequence libraries were prepared using the NEBNext Ultra II Directional RNA Library Prep Kit for Illumina (New England Biolabs, Ipswich) and sequenced on the NextSeq 550 (Illumina) with NextSeq 500/550 High Output Kit V2 (75 CYS, Illumina, San Diego, CA). Reads were aligned to the GRCm38 v96 Ensembl *Mus musculus* genome using STAR v.2.7.0f (28) with default parameters. Downstream RNA-seq data analysis was performed using the statistical software R (29). Differential gene expression analysis was performed with the R-package DEseq2 v1.24.03232. Genes with a Benjamini and Hochberg adjusted $P \leq 0.05$ after correcting for multiple testing (5% false discovery rate) were regarded as statistically significantly regulated. Gene regulation and expression were investigated in 153 mouse homologous genes (out of 158 human gene markers) curated based on previous reports of association with human HCC (30–33).

MASLD Human Proximity Score

The MASLD Human Proximity Score (MHPS) ranking system, developed by the LITMUS Consortium (https://litmus-project.eu/), was applied to rank the current CDAA-HFD models (3, 6, 12, and 20 wk on diet, respectively) against a total of 39 established MASLD rodent models and CCl_4 as a positive control for fibrosis, as described in detail by Vacca et al. (34). The MHPS ranking system is a bioinformatic pipeline integrating metabolic phenotype data, liver histology, and liver transcriptome benchmarked against human disease to create a score reflecting proximity to human MASH outcome. Histological scoring data from the CDAA-HFD mouse was derived using the GHOST automated deep learning-based image analysis and thoroughly reviewed by expert liver pathologists. Histology data as well as corresponding phenotypic data (body weight, liver weight, plasma ALT, AST, and TG) and transcriptomics data were integrated into the bioinformatic pipeline, yielding a score in the MHPS ranking system. This unbiased scoring method provides a dual ranking based on the ability of the rodent model to induce metabolic or MASH-fibrotic outcomes. The bioinformatic pipeline integrates the three layers of metabolic phenotype data, liver histology, and liver transcriptomics. The score from each layer is combined into the final metabolic- or MASH-fibrosis-related MHPS final ranking, summarizing the rodent model's resemblance to corresponding human MASLD outcomes.

Statistics

Except for deep learning-based image analysis and RNA sequencing (described earlier), data were analyzed using GraphPad Prism v9.0.2 software (GraphPad, La Jolla, CA). All results are shown as means ± SE. Dunnett's test one- or two-factor linear model with interaction was used for all other statistical analyses. A P value less than 0.05 was considered statistically significant.

RESULTS

GHOST Deep Learning-Based Automated Histopathological Scoring in CDAA-HFD Mice

Liver biopsy sections stained with HE and PSR were used for the detection of central veins and portal triads (Fig. 1, *A*, *B*, *E*, and *F*), enabling subsequent segmentation of zones for NAS and fibrosis histopathological scoring. Relevant cell types (hepatocytes, inflammatory cells, and ballooned hepatocytes) were identified using HE-stained sections (Fig. 1, *A*–*C*). Inflammatory foci were defined and segmented as clusters of three or more adjacent inflammatory cells (Fig. 1*D*). A test set of 103 liver biopsies (93 CDAA-HFD mice and 10 chow mice) was employed for designing and validating the GHOST application. For these biopsies, histopathological scores derived from the GHOST AI pipeline were compared with manual NAS scoring assessed by expert histopathologists. The reliability of the GHOST application was assessed using Cohen's kappa coefficient, demonstrating high concordance between automated and manual NAS scoring (Fig. 1*I*, Cohen's kappa value: 0.85). Collagen fibers visualized by PSR staining were segmented according to anatomical architecture, i.e., sinusoidal or periportal fibrosis (Fig. 1*G*), further enabling the segmentation of fibers forming bridges and branch points (Fig. 1*H*). Based on these segmentations, the fibrosis stage was computed and validated on the test set of 288 mouse liver biopsies, demonstrating a high degree of agreement between automated and manually scored samples (Fig. 1*J*, Cohen's kappa value: 0.81). In addition, the GHOST application was used for additional quantitative assessment of histopathological scoring variables, including steatosis (relative number of hepatocytes with lipid droplets), lobular inflammation (number of inflammatory foci), and fibrosis (sinusoidal and periportal fibrosis).

Disease Progression in CDAA-HFD Mice

Parameters of MASH were evaluated after 3–20 wk of CDAA-HFD feeding and compared with mice fed a chow diet for 20 wk (Fig. 2*A*). Groups (3w and 12w) ran in parallel while 6w and 20w groups ran independently. CDAA-HFD mice demonstrated lower weight, compared with chow-fed animals (Fig. 2*B*; CDAA-HFD 20w, 24 ± 0.2 g; chow, 29 ± 0.3 g, $P < 0.001$). CDAA-HFD mice demonstrated robust hepatomegaly (Fig. 2*C*; CDAA-HFD 20w, 2.0 ± 0.1 g; chow, 1.2 ± 0.1 g, $P < 0.001$). Compared with chow controls, plasma markers of liver injury (ALT, AST) were significantly increased at all timepoints (Fig. 2, *D* and *E*, $P < 0.001$), peaking after 6 wk of CDAA-HFD feeding. Twelve weeks of CDAA-HFD diet feeding reduced lean tissue mass (25%) as well as fasting plasma insulin, HOMA-IR, and glucose AUC in an intraperitoneal glucose tolerance test (IPGTT) (Supplemental Fig. S1, *A*–*F*, $P < 0.001$). Levels of plasma TG and TC were decreased after 12 wk of CDAA-HFD feeding while plasma TIMP-1, plasma PIIINP, liver triglycerides (TG), liver total cholesterol (TC), and liver hydroxyproline (HP) were increased (Supplemental Fig. S1, *G*–*M*, $P < 0.001$). Histological analyses indicated rapid onset of MASH (NAS = 6) after 3 wk of CDAA-HFD feeding (Fig. 2*F*, $P < 0.001$). This was also reflected by the rapid induction of severe steatosis (score 3) and lobular inflammation (score 3) (Fig. 2*G*, $P < 0.001$). Ballooning degeneration was absent in CDAA-HFD mice, irrespective of the feeding period employed (Fig. 2*G*). Mild to moderate fibrosis (*stages F1–2*) was evident from *week 6* and progressed to advanced fibrosis (*stage F3*) in all animals from *week 12* and onward (Fig. 2*F*, $P < 0.001$). Histomorphometric analyses supported accelerated disease progression in CDAA-HFD mice. Accordingly, the CDAA-HFD mice demonstrated significantly increased quantitative histological markers of steatosis (% hepatocytes with lipid droplets, Fig. 2*H*, $P < 0.001$; % area of lipids, Fig. 2*M*, $P < 0.001$) lobular inflammation (number of inflammatory foci, Fig. 2*I*, $P < 0.001$; % area of galectin-3, Fig. 2*N*, $P < 0.001$) from *week 3* and onward. α-SMA, an early marker of HSC activation and fibrogenesis3838, was gradually increased from *weeks 3* to *12* (Fig. 2*O*, $P < 0.001$) and remained stable thereafter. Markers of fibrosis (% area of periportal fibrosis, sinusoidal fibrosis; % area of PSR and Col1a1) showed progressive increases over the entire study period, however, most markedly after 12 wk of CDAA-HFD feeding (Fig. 2, *J*, *K*, *L*, and *P*, $P < 0.001$). The total content of individual quantitative histological markers is shown in Supplemental Fig. S5*A*.

Transcriptome Signatures in CDAA-HFD Mice

Hepatic global gene expression signatures in CDAA-HFD fed mice clearly separated from chow-fed controls, as shown by the PCA plot of the 500 most variables (Fig. 3*A*). There was an excessive number of differentially expressed genes (DEGs) detected after 3 wk on diet ($n = 9{,}751$), which increased further with extended duration of CDAA-HFD feeding (Fig. 3*B*). Considerable overlap between liver transcriptome signatures was observed in mice fed the CDAA-HFD for 3–20 wk (Fig. 3*C*). At all timepoints, CDAA-HFD mice displayed a widespread increase in the expression of seven defined gene categories, i.e., inflammation, hepatocellular injury and extracellular matrix (ECM) organization as compared with chow-fed controls. Less pronounced regulations were observed for genes associated with glucose, bile, and lipid metabolism as well as ER stress (Fig. 3*D*). At all timepoints, CDAA-HFD feeding promoted widespread downregulation of genes related to cholesterol biosynthesis. The RNA sequencing data were examined for potential regulations in genes encoding drug targets relevant in the subsequent pharmacological studies. Compared with chow controls, CDAA-HFD feeding progressively reduced *Ppar-a* expression but upregulated *Ppard* and *Pparg* (Fig. 3*D*). CDAA-HFD feeding also significantly decreased *Acaca* (*Acc1*), *Acacb* (*Acc2*), *Nr1h4* (*Fxr*), and *Thrb* (Fig. 3*D*). Hepatic *Glp1r* expression was undetectable in both chow-fed controls and CDAA-HFD mice (data not shown).

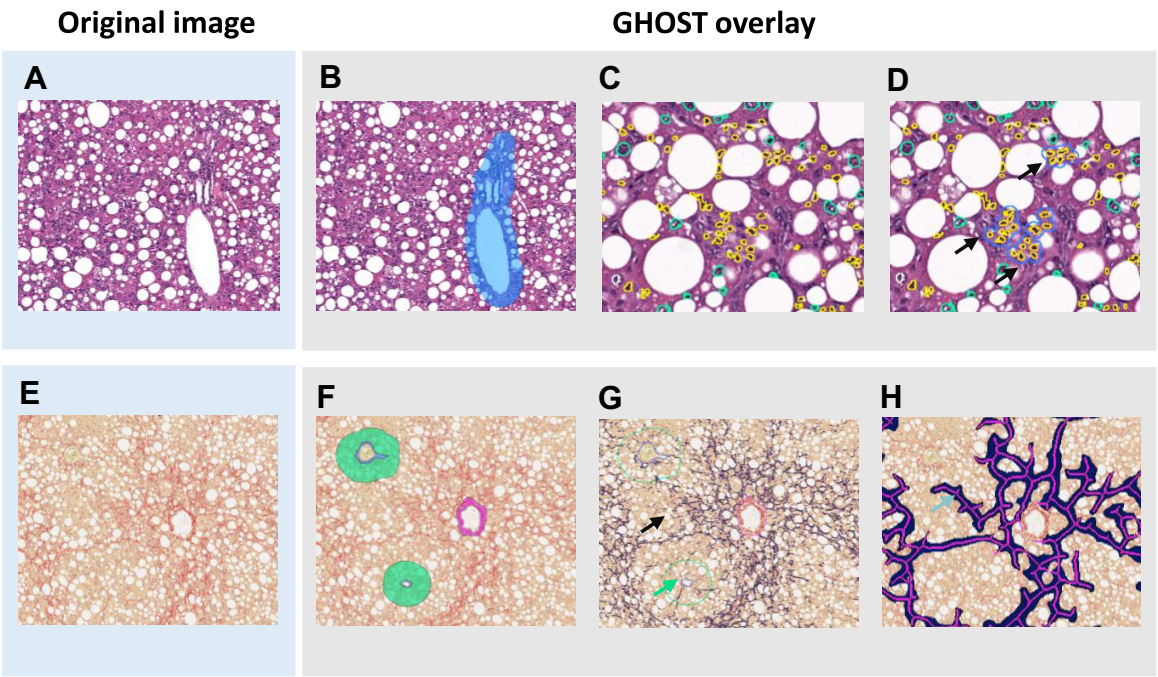

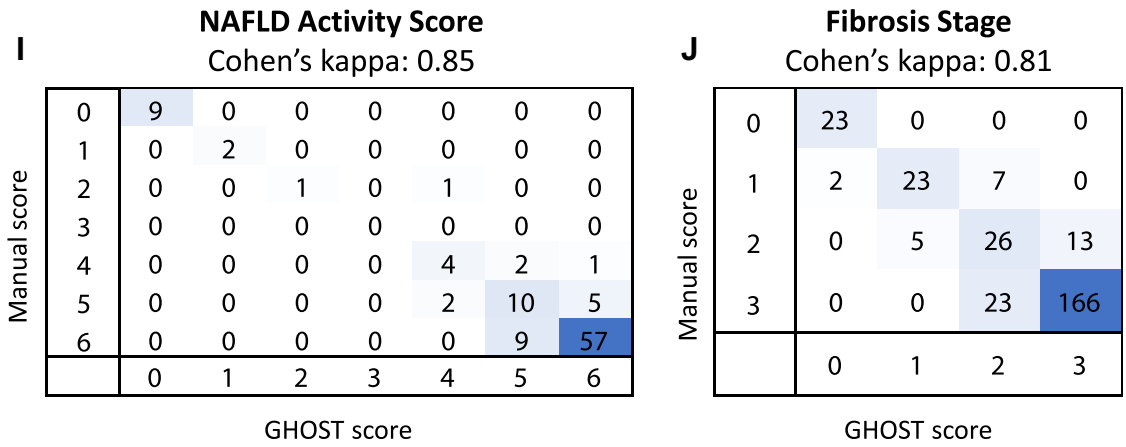

Figure 1. Deep learning-based assessment of NAFLD Activity Score (NAS) and fibrosis stage of the liver in CDAA-HFD mice. *A*: steatosis, inflammation, and hepatocyte ballooning degeneration scores were evaluated on hematoxylin-eosin (HE) stained slides. *B*: deep learning-based detection (GHOST application) of portal tract (blue) at ×10 magnification. *C*: deep learning detected nuclei of hepatocytes with lipid droplets (green), hepatocytes without lipids (white), and inflammatory cells (yellow) at ×20 magnification. *D*: by postprocessing, inflammatory foci were defined as a cluster of >3 inflammatory cells (blue). Scores were calculated based on simple threshold. *E*: fibrosis stage was evaluated on scanned picrosirius red (PSR)-stained slides. *F*: deep learning-based detection of portal tract (blue) and central veins (pink) at ×10 magnification. The boundary of the periportal zone was defined as 100 µm from the portal tract (green). *G*: detection of collagen fibers (dark blue) in the periportal (black arrow) and sinusoidal (green arrow) zones. Fibrosis was detected using the linear Bayesian image analysis method, and different measures of collagen fiber fragment size and shape was used to predict bridging. *H*: detection of bridging fibrosis (pink), bridging zones (blue), and branch points (gray arrow). Bridging was detected using the threshold image analysis method based on a polynomial local linear filter feature. Correlation of manual vs. GHOST-based assessment of NAFLD Activity Score (NAS; *I*) and fibrosis stage (*J*). CDAA-HFD, choline-deficient L-amino acid defined-high-fat diet; GHOST, Gubra Histopathological Objective Scoring Technology; NAFLD, nonalcoholic fatty liver disease.

CDAA-HFD Mice Develop Tumors with HCC Gene Expression Profiles

Macroscopic evaluation of surface tumors revealed tumor development only after 20 wk of CDAA-HFD induction (CDAA-HFD 20w, 92% of mice with tumors; chow, 0% of mice with tumors, $P < 0.001$) (Supplemental Fig. S2). This was supported by analysis of a set of human HCC-associated oncogenes and tumor suppressor genes (35), with significant changes being manifest already after 3 wk on the CDAA-HFD diet (Supplemental Fig. S3).

MASLD Human Proximity Score Ranking of the CDAA-HFD Mouse Model

To assess the performance of the CDAA-HFD mouse model in recapitulating human MASH, we applied the MASLD Human Proximity Score (MHPS) (34). The bioinformatics

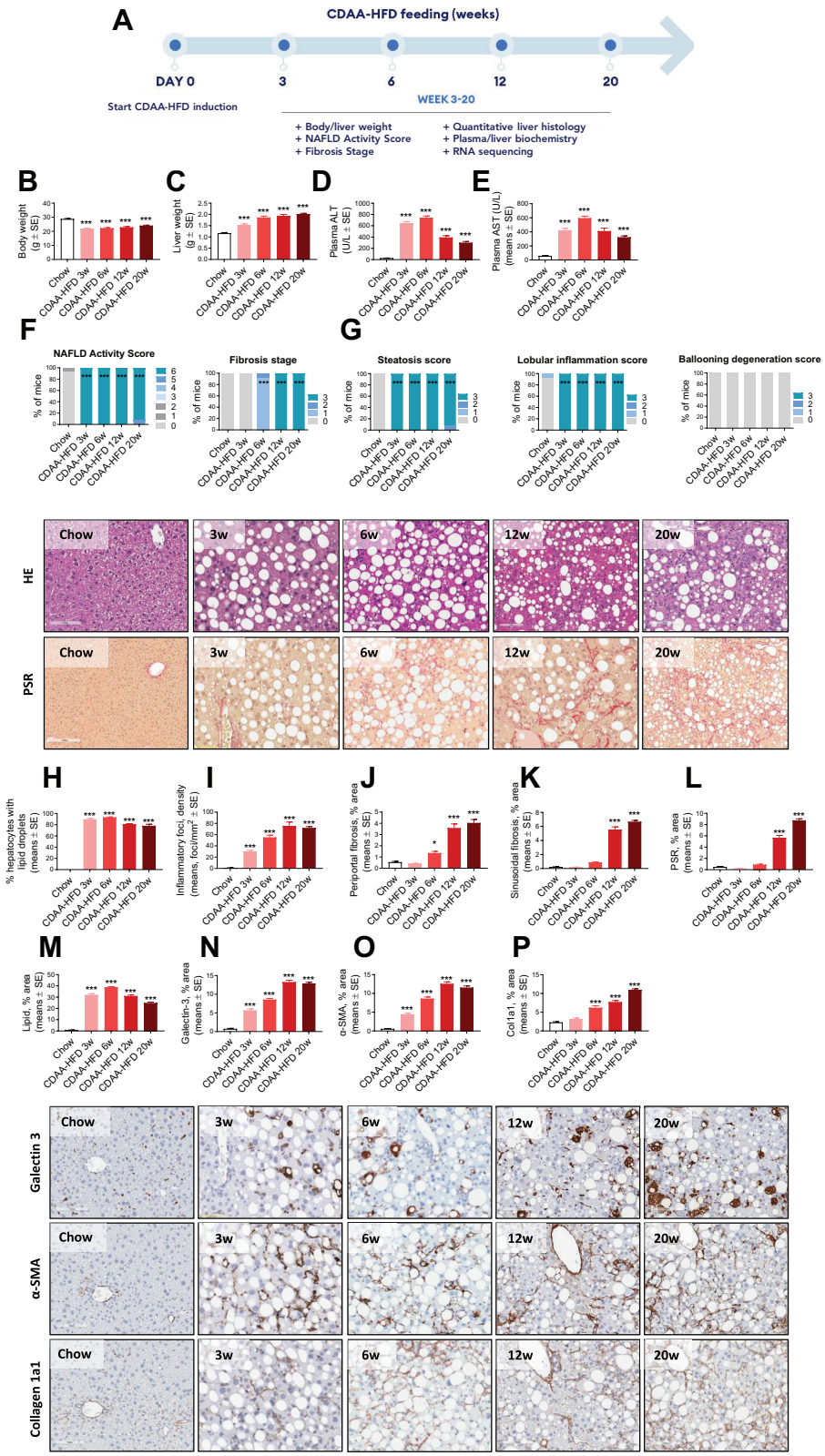

Figure 2. CDAA-HFD mice show progressive development of severe MASH with advanced fibrosis. Mice were fed the CDAA-HFD diet for 3–20 wk ($n = 12$ per group). Chow-fed mice ($n = 8$) served as healthy controls. *A*: study outline. *B*: terminal body weight. *C*: liver weight. *D*: plasma ALT. *E*: plasma AST. *F*: NAFLD Activity Score (NAS) and fibrosis stage. *G*: steatosis, lobular inflammation, and ballooning degeneration scores. *H–P*: GHOST-based histomorphometrics on histopathological scoring variables of lipid-laden hepatocytes (*H*), inflammatory foci (*I*), and periportal/sinusoidal fibrosis (*J* and *K*), % area of picrosirius red (PSR) (*L*), proportionate (%) area of lipids (*M*), % area of inflammation (galectin-3; *N*), % area of α-SMA (fibrogenesis marker; *O*), and % area of Col1a1 (*P*). See Supplemental Fig. S5 for total liver histological marker levels. *Middle*: hematoxylin-eosin (HE) and PSR staining illustrating the development of steatosis and fibrosis in CDAA-HFD mice (scale bar, 100 μm). *Bottom*: representative photomicrographs of galectin-3, α-SMA, and Col1a1 immunostainings (scale bar, 100 μm). $*P < 0.05$, $***P < 0.001$ vs. chow (Dunnett's test one-factor linear model). α-SMA; α-smooth muscle action; ALT, alanine aminotransferase; AST, aspartate aminotransferase; CDAA-HFD, choline-deficient L-amino acid defined-high-fat diet; GHOST, Gubra Histopathological Objective Scoring Technology; MASH, metabolic dysfunction-associated steatohepatitis; NAFLD, nonalcoholic fatty liver disease.

pipeline consists of a dual ranking system yielding a MASH-fibrotic ranking and metabolic ranking, respectively, based on the assessment of metabolic phenotype (Phenotype Human Proximity Score, PHPS), histological features (Histology Human Proximity Score, HHPS), and transcriptomic profiles [(Drug Set Enrichment Analysis, DSEA) Human Proximity Score, DHPS], benchmarked against human MASH. The highest-ranking models for both MASH-fibrosis and metabolic resemblance were all based on GAN diet feeding. The CDAA-HFD mouse aligned within the spectrum

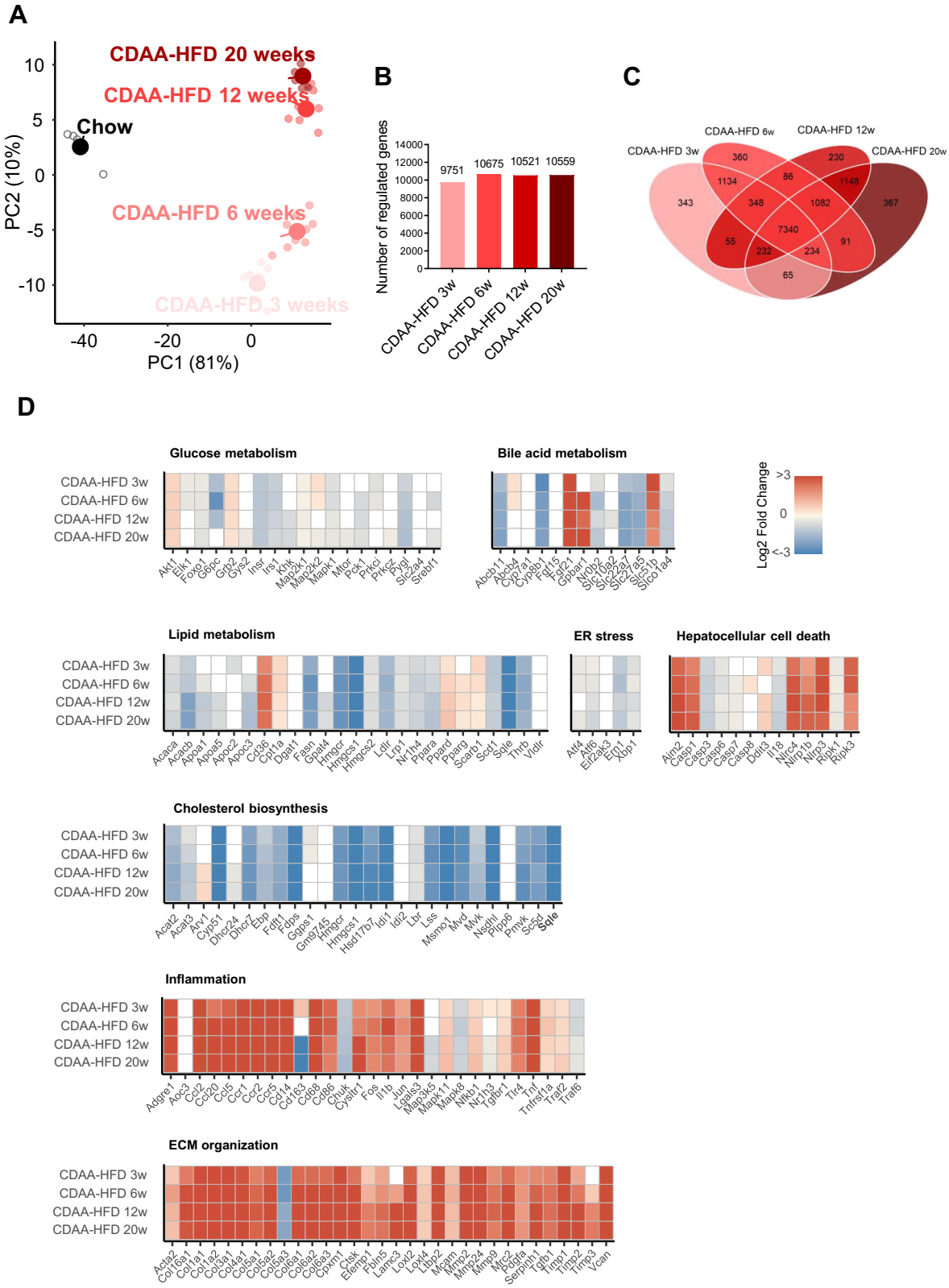

Figure 3. Changes in MASH-associated hepatic gene expression signatures in response to extended CDAA-HFD feeding. *A*: principal component analysis (PCA) of samples based on the top 500 most variable gene expression levels. *B*: total number of differentially regulated genes compared with chow. *C*: Venn diagram depicting shared and separate differentially expressed genes in each group. *D*: heatmaps illustrating changes in MASH and fibrosis-associated candidate gene expression compared with chow mice. Color gradients in heatmaps indicate significantly upregulated (red color) or downregulated (blue color) gene expression (log2-fold change, false discovery rate < 0.05). Genes with nonsignificant changes are marked in white. CDAA-HFD, choline-deficient L-amino acid defined-high-fat diet; MASH, metabolic dysfunction-associated steatohepatitis.

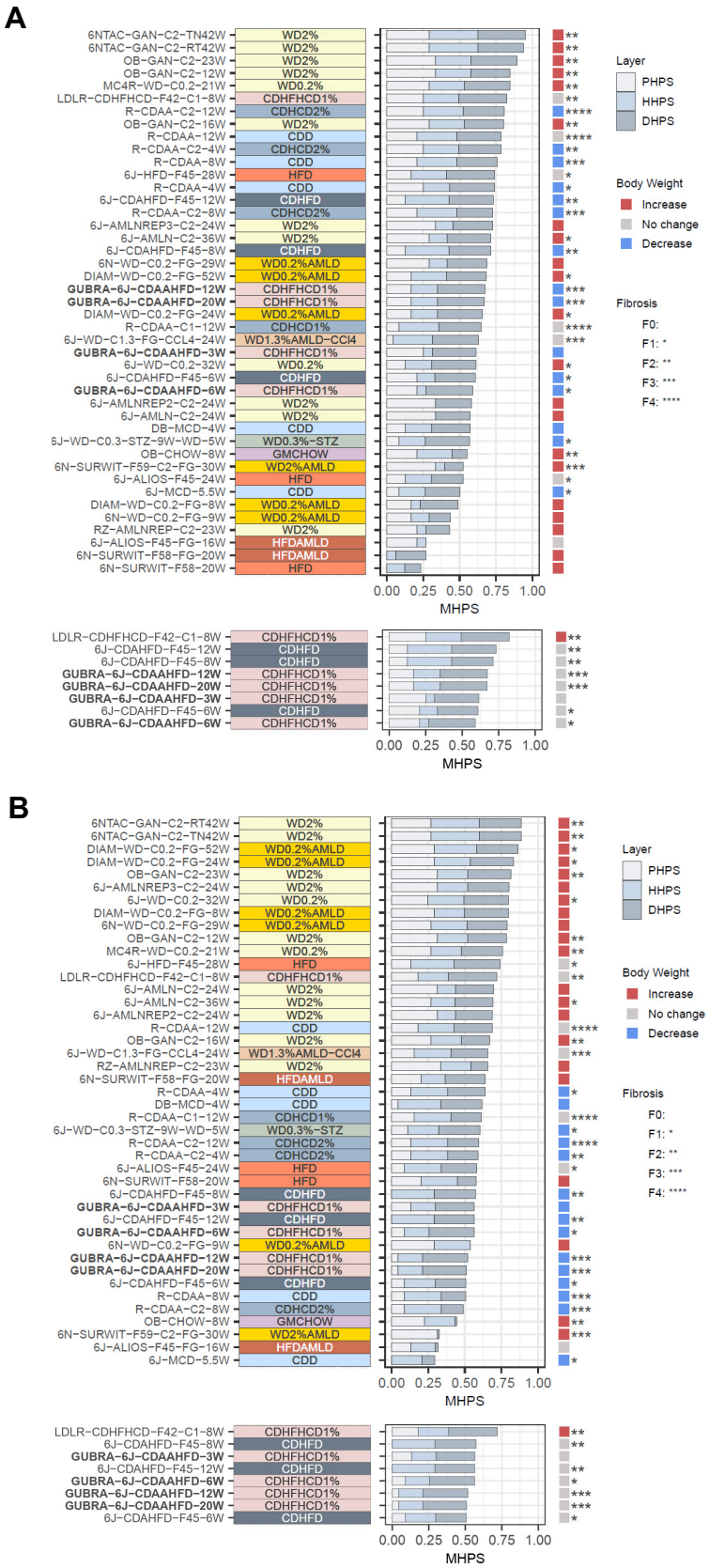

Figure 4. CDAA-HFD model ranking compared with other MASLD models as assessed by the MASLD Human Proximity Score (MHPS). The final scoring consists of three layers assessing the resemblance to human phenotypic outcomes (Phenotype Human Proximity Score, PHPS), histological features (Histology Human Proximity Score, HPPS), and transcriptomic profiles (DSEA Human Proximity Score, DHPS). The contribution of each component is indicated by the length of each stack in the horizontal bars. *A:* MASH-fibrotic ranking assessing progressive MASLD relevance. *B:* metabolic ranking based on the examined models' ability to induce MASLD metabolic outcomes. The current model, GUBRA-6J-CDAAHFD-W3 to W20, is highlighted in bold. Lower panels compare CDAA-HFD based model only. CDAA-HFD, choline-deficient L-amino acid defined-high-fat diet; MASLD, Metabolic dysfunction-associated steatotic liver disease; MASH, metabolic dysfunction-associated steatohepatitis.

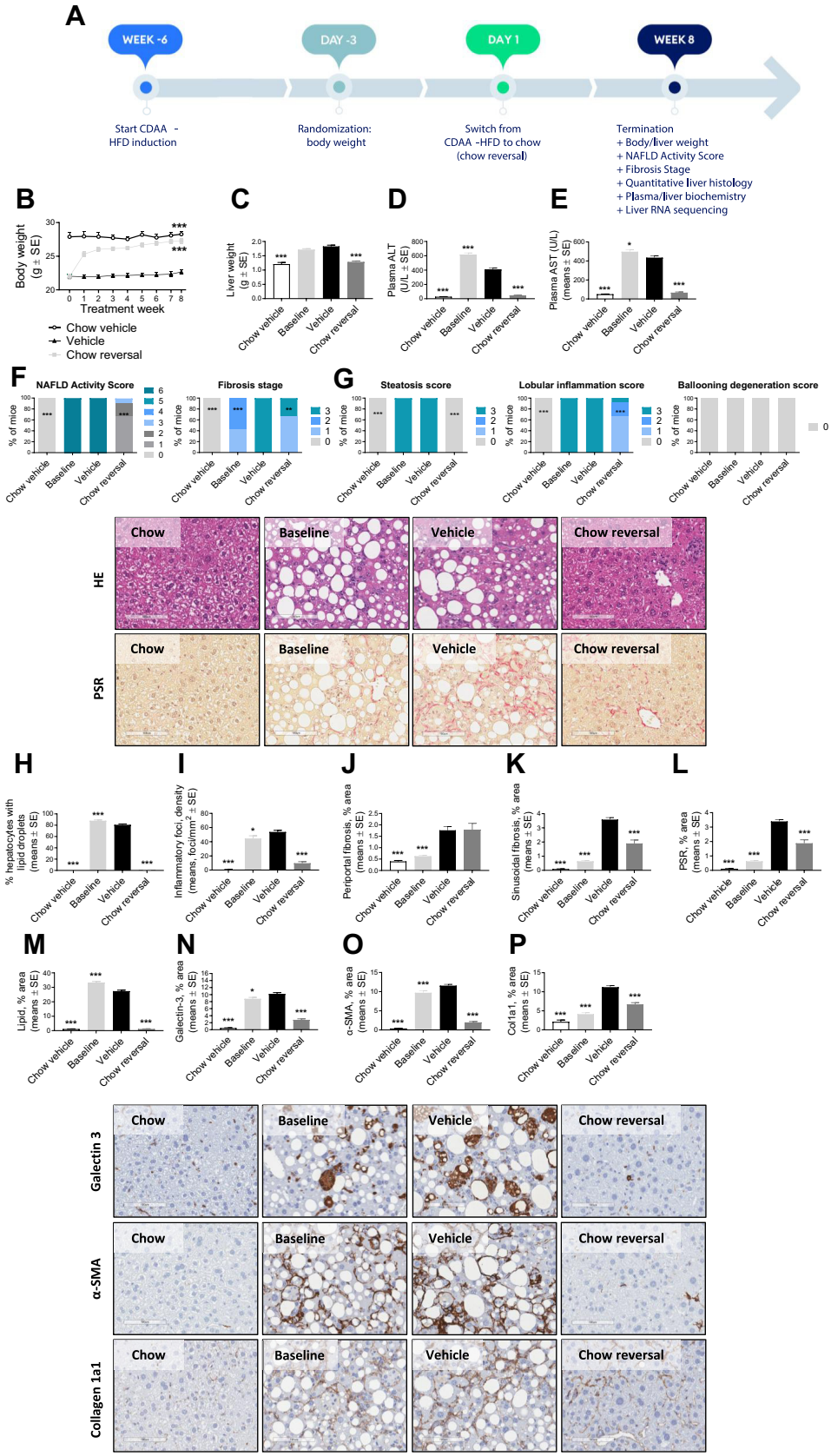

Figure 5. Dietary intervention improves hallmarks of MASH without alleviating fibrosis. Mice were fed the CDAA-HFD diet ($n = 12$ per group) or chow ($n = 8$) for 6 wk whereafter animals were switched to chow diet or remained on CDAA-HFD diet for 8 more weeks. The baseline group was terminated on *study day 1*. *A:* study outline. *B:* body weight profile over the treatment period. *C:* liver weight. *D:* plasma ALT. *E:* plasma AST. *F:* NAFLD Activity Score (NAS) and fibrosis stage. *G:* steatosis, lobular inflammation, and ballooning degeneration scores. *H–P*: GHOST-based histomorphometrics on histopathological scoring variables of lipid-laden hepatocytes (*H*), inflammatory foci (*I*), and periportal/sinusoidal fibrosis (*J* and *K*), proportionate (%) area of lipids (*L*), % area of inflammation (galectin-3; *M*), % area of α-SMA (fibrogenesis marker; *N*), % area of picrosirius red (PSR) (*O*), and % area of Col1a1 (*P*). See Supplemental Fig. S5 for total liver histological marker levels. *Middle*: hematoxylin-eosin (HE) and PSR staining illustrating the development of steatosis and fibrosis in CDAA-HFD mice (scale bar, 100 μm). *Bottom*: representative photomicrographs of galectin-3, α-SMA, and Col1a1 immunostainings (scale bar, 100 μm). $*P < 0.05$, $**P < 0.01$, $***P < 0.001$ vs. chow-fed controls (Dunnett's test one-factor linear model). α-SMA; α-smooth muscle action; ALT, alanine aminotransferase; AST, aspartate aminotransferase; CDAA-HFD, choline-deficient L-amino acid defined-high-fat diet; GHOST, Gubra Histopathological Objective Scoring Technology; MASH, metabolic dysfunction-associated steatohepatitis; NAFLD, nonalcoholic fatty liver disease.

of the well-established choline-deficient MASLD models but featured more advanced fibrosis (*stage F3*, bridging fibrosis) compared with other CDAA-HFD based models. When assessing MASH-fibrosis ranking (Fig. 4*A*), the CDAA-HFD models (3, 6, 12, or 20 wk on diet) revealed a significant degree of similarity to human MASH fibrotic-related outcomes as reflected by intermediate MHPS scores. The model displays high similarity within DHPS, being relevant for the evaluation of intrahepatic targets. Notably, CDAA-HFD models generally scored lower in the metabolic ranking (Fig. 4*B*), emphasizing

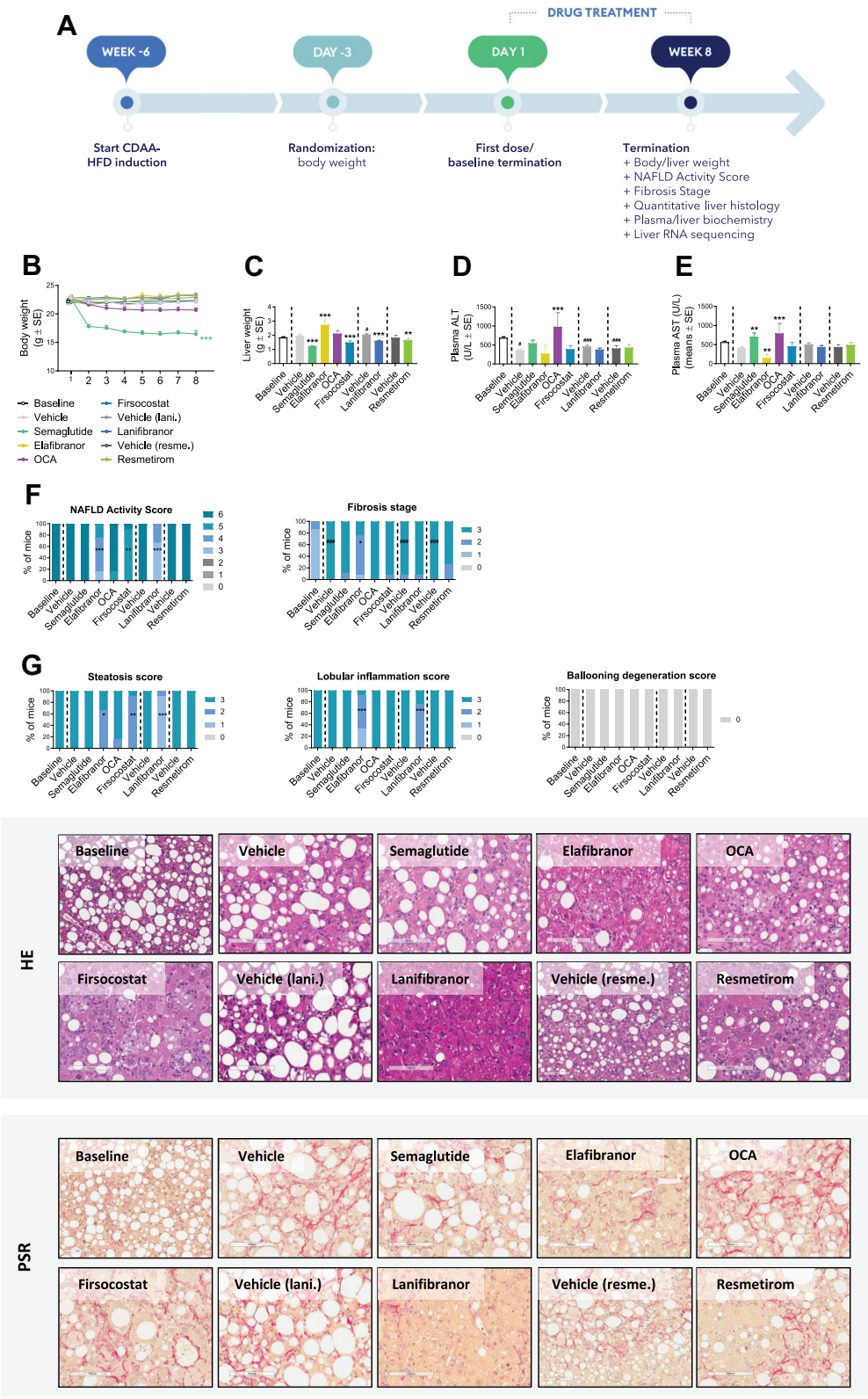

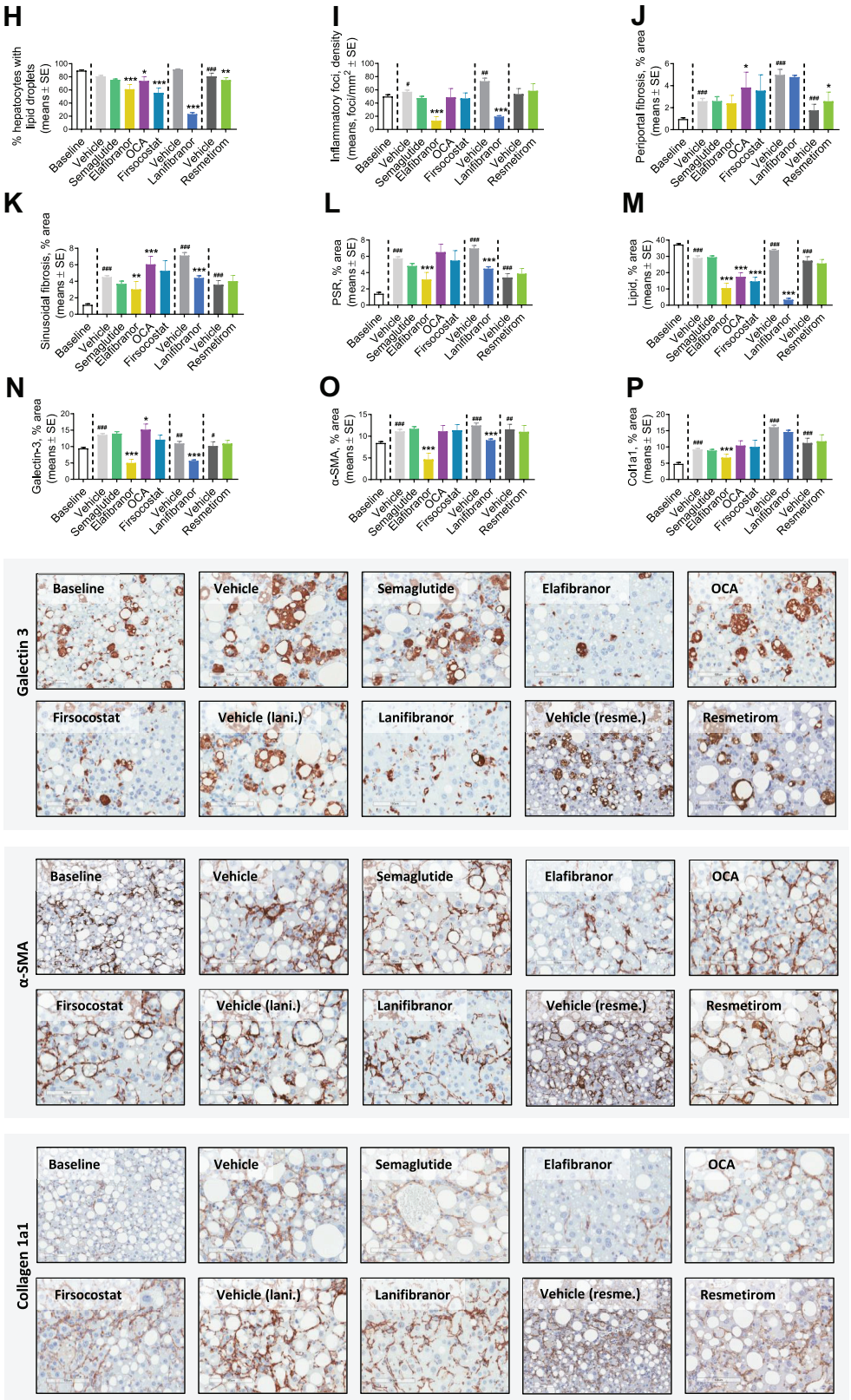

Figure 6. *Continued.*

known limitations (nonobese phenotype, loss of lean tissue mass, lack of glucose intolerance, and insulin resistance) in the human translatability of these models.

Dietary Treatment Intervention Improves Hallmarks of MASH and Fibrosis in CDAA-HFD Mice

Dietary intervention (chow reversal) was characterized in the context of manifest fibrosis (treatment intervention). CDAA-HFD mice were switched to normal chow after 6 wk of CDAA-HFD feeding and remained on chow for 8 wk (Fig. 5*A*). Compared with vehicle controls, dietary intervention promoted almost complete recovery of CDAA-HFD induced body weight loss (Fig. 5*B*; vehicle, 23 ± 0.4 g; chow reversal, 27 ± 0.4 g; chow vehicle 28 ± 0.4 g, $P < 0.001$). Hepatomegaly was normalized by dietary intervention (Fig. 5*C*; vehicle, 1.8 ± 0.1 g; chow reversal, 1.3 ± 0.1 g; chow vehicle, 1.2 ± 0.1 g, $P < 0.001$) and elevated plasma transaminases were fully reversed (Fig. 5, *D* and *E*, $P < 0.001$). Metabolic benefits of dietary intervention were paralleled by complete reversal of steatosis and robust improvements in lobular inflammation (Fig. 5, *F* and *G*, $P < 0.001$). Dietary intervention consistently improved the fibrosis stage (Fig. 5*F*; vehicle, $F = 3$, 12 out of 12 mice; chow reversal, $F = 1$, 8/12 mice, $F = 3$, 4/12 mice, $P < 0.01$). Furthermore, dietary intervention reduced liver HP levels (Supplemental Fig. S4*A*, $P < 0.001$). Improvements in histopathological scores were supported by corresponding improvements in quantitative histological endpoints. Accordingly, dietary intervention led to pronounced improvements in histological markers of steatosis (% hepatocytes with lipid droplets, Fig. 5*H*, $P < 0.001$; % area of lipids, Fig. 5*M*, $P < 0.001$) and inflammation (number of inflammatory foci, Fig. 5*I*, $P < 0.001$; % area of galectin-3, Fig. 5*N*, $P < 0.001$) as compared with vehicle controls. Chow reversal normalized α-SMA levels (Fig. 5*O*, $P < 0.001$) and reduced the percent area of sinusoidal fibrosis, PSR, and Col1a1 (Fig. 5, *K*, *L*, and *P*, $P < 0.001$), while not improving the percent area of periportal fibrosis (Fig. 5*J*, $P > 0.05$). The total content of individual quantitative histological markers is shown in Supplemental Fig. S5*B*.

Differential Outcomes of Drug Treatment Intervention in CDAA-HFD Mice

Treatment was initiated after 6 wk of CDAA-HFD feeding to evaluate therapeutic benefits of semaglutide, elafibranor, OCA, firsocostat, lanifibranor, and resmetirom in the context of manifest fibrosis (treatment intervention) (Fig. 6*A*). Compared with baseline, vehicle-dosed CDAA-HFD mice demonstrated progressive fibrosis, as indicated by increased fibrosis stage (Fig. 6*F*, $P < 0.001$) and supported by quantitative histological markers of fibrosis (Fig. 6, *J*, *K*, *L*, *O*, and *P*, $P < 0.001$); while NAS, steatosis- and lobular inflammation scores were unchanged compared with baseline (Fig. 6, *F* and *G*, $P > 0.05$). Semaglutide markedly reduced body weight (−25%), while elafibranor, OCA, firsocostat, lanifibranor, and resmetirom had no significant effect on body weight (Fig. 6*B*; vehicle, 22 ± 0.4 g; semaglutide, 16 ± 0.7 g, $P < 0.001$). OCA increased plasma ALT (Fig. 6*D*, $P < 0.05$) and OCA and semaglutide increased AST (Fig. 6*E*, $P < 0.01$) compared with corresponding vehicle-dosed controls. Elafibranor decreased plasma AST (Fig. 6*E*, $P < 0.001$). Firsocostat, lanifibranor, and resmetirom did not alter levels of plasma ALT and AST (Fig. 6, *D* and *E*, $P > 0.05$). Semaglutide, firsocostat, lanifibranor, and resmetirom improved hepatomegaly compared with corresponding vehicle-dosed CDAA-HFD controls (Fig. 6*C*, $P < 0.001$). Elafibranor increased liver weight, while OCA had no effect. Semaglutide, elafibranor, firsocostat, and lanifibranor reduced liver HP levels (Supplemental Fig. S4*B*, $P < 0.001$). Elafibranor, firsocostat, and lanifibranor significantly improved NAS (Fig. 6*F*; vehicle, NAS = 6, 12 out of 12 mice; elafibranor, NAS = 3, 2/12 mice, NAS = 4, 7/12 mice, NAS = 5, 3/12 mice, $P < 0.001$; firsocostat, NAS = 5, 10/11 mice, NAS = 6, 1/11 mice, $P < 0.01$; vehicle (lani.), NAS = 6, 12/12 mice; lanifibranor, NAS = 3, 8/12 mice, NAS = 4, 4/12 mice, $P < 0.001$) due to improvements in steatosis and lobular inflammation scores (Fig. 6*G*, $P < 0.001$). Elafibranor improved fibrosis stage (Fig. 6*F*; vehicle, $F = 3$, 12 out of 12 mice; elafibranor, $F = 1$, 1/12 mice, $F = 2$, 8/12, $F = 3$, 3/12 mice, $P < 0.05$). Semaglutide, lanifibranor, OCA, firsocostat, and resmetirom did not improve fibrosis stage compared with corresponding vehicle-dosed controls (Fig. 6*F*, $P > 0.05$). In agreement with histopathological scores, elafibranor and lanifibranor significantly reduced quantitative histological markers of steatosis (% hepatocytes with lipid droplets, Fig. 6*H*, $P < 0.001$; % area of lipids, Fig. 6*M*, $P < 0.001$), inflammation (number of inflammatory foci, Fig. 6*I*, $P < 0.001$; % area of galectin-3, Fig. 6*N*, $P < 0.001$) and fibrosis (% area of α-SMA, Fig. 6*O*, $P < 0.001$; % area of sinusoidal fibrosis, Fig. 6*K*, $P < 0.001$; % area of PSR, Fig. 6*L*, $P < 0.001$), but not periportal fibrosis and Col1a1 (Fig. 6, *J* and *P*, $P > 0.05$). OCA and firsocostat reduced quantitative histological markers of steatosis, but not markers of inflammation and fibrosis. Semaglutide and resmetirom had little or no effect on liver histomorphometry. The total content of individual quantitative histological markers is shown in Supplemental Fig. S5*C*.

Greater Efficacy of Semaglutide and Lanifibranor Prevention Therapy in CDAA-HFD Mice

Semaglutide and lanifibranor monotherapy was characterized in CDAA-HFD mice with manifest MASH without established fibrosis at baseline (preventative intervention). To this end, treatment was initiated after 3 wk of CDAA-HFD feeding and continued for 9 wk (Fig. 7*A*). There was no difference

Figure 6. Treatment intervention with semaglutide and lanifibranor improves aspects of MASH but not fibrosis stage. Mice ($n = 10$–12 per group) were fed the CDAA-HFD diet for 6 wk whereafter drug treatment commenced and was maintained for 8 wk. The baseline group was terminated at *study day 1*. *A*: study outline. *B*: body weight profile over the treatment period. *C*: liver weight. *D*: plasma ALT. *E*: plasma AST. *F*: NAFLD Activity Score (NAS) and fibrosis stage. *G*: steatosis, lobular inflammation, and ballooning degeneration scores. hematoxylin-eosin (HE) and picrosirius red (PSR) staining illustrating the development of steatosis and fibrosis in CDAA-HFD mice (scale bar, 100 μm). *H*–*P*: GHOST-based histomorphometrics on histopathological scoring variables of lipid-laden hepatocytes (*H*), inflammatory foci (*I*), and periportal/sinusoidal fibrosis (*J* and *K*), % area of PSR (*L*), proportionate (%) area of lipids (*M*), % area of inflammation (galectin-3; *N*), % area of α-SMA (fibrogenesis marker; *O*), and % area of Col1a1 (*P*). See Supplemental Fig. S5 for total liver histological marker levels. Representative photomicrographs of galectin-3, α-SMA, and Col1a1 immunostainings (scale bar, 100 μm). *$P < 0.05$, **$P < 0.01$, ***$P < 0.001$ vs. corresponding vehicle and #$P < 0.05$, ##$P < 0.01$, ###$P < 0.001$ vs. Baseline (Dunnett's test one-factor linear model). α-SMA; α-smooth muscle action; ALT, alanine aminotransferase; AST, aspartate aminotransferase; CDAA-HFD, choline-deficient L-amino acid defined-high-fat diet; GHOST, Gubra Histopathological Objective Scoring Technology; MASH, metabolic dysfunction-associated steatohepatitis; NAFLD, nonalcoholic fatty liver disease.

between baseline groups from semaglutide and lanifibranor treatment arm and baseline groups were therefore pooled. Compared with baseline, vehicle-dosed CDAA-HFD mice showed worsening of fibrosis (Fig. 7*F*, $P < 0.001$) and increased quantitative histological markers of inflammation and fibrosis (Fig. 7, *I–P*, $P < 0.001$). Composite NAS as well steatosis and lobular inflammation scores were unchanged. Although semaglutide significantly reduced body weight in CDAA-HFD mice, lanifibranor was weight-neutral in the model (Fig. 7*B*; Veh-SC, 22 ± 0.3 g; semaglutide, 17 ± 0.3 g, $P < 0.001$; Veh-PO, 22 ± 0.4 g; lanifibranor, 21 ± 0.4 g, $P > 0.05$). Neither compound influenced plasma ALT and AST levels (Figs. 7*D* and 5*E*, $P > 0.05$). Both semaglutide and lanifibranor improved hepatomegaly (Fig. 7*C*, $P < 0.001$). Lanifibranor and semaglutide reduced liver HP ($P < 0.001$) (Supplemental Fig. S4*C*). Lanifibranor, but not semaglutide, improved NAS (Fig. 7*F*; Veh-PO, NAS = 6, 12 out of 12 mice; lanifibranor, NAS = 3, 8/11 mice, NAS = 4, 3/11 mice; $P < 0.001$) driven by improvements in both steatosis and lobular inflammation scores. Notably, both semaglutide and lanifibranor improved fibrosis stage (Fig. 7*F*; Veh-PO, $F = 3$, 12 out of 12 mice; lanifibranor, $F = 1$, 1/11 mice, $F = 2$, 8/11 mice, $F = 3$, 2/11 mice, $P < 0.001$; Veh-SC, $F = 3$, 12/12 mice; semaglutide, $F = 2$, 8/12 mice, $F = 3$, 4/12 mice, $P < 0.01$). The benefits on histopathological scores were supported by corresponding improvements in quantitative histological endpoints. Accordingly, semaglutide reduced % hepatocytes with lipid droplets (Fig. 7*H*, $P < 0.001$), but did not improve % area of lipids (Fig. 7*M*, $P > 0.05$) compared with the vehicle. Semaglutide did not influence the number of inflammatory foci and % area of galectin-3 (Fig. 7, *I* and *N*, $P > 0.05$), but reduced % area of sinusoidal fibrosis (Fig. 7*K*, $P < 0.001$) and total-section PSR staining (Fig. 7*L*, $P < 0.001$). In contrast, semaglutide increased % area of α-SMA (Fig. 7*O*, $P < 0.001$). In comparison, lanifibranor markedly reduced markers of steatosis (% hepatocytes with lipid droplets, Fig. 7*H*, $P < 0.001$; % area of lipids, Fig. 7*M*, $P < 0.001$) and lobular inflammation (number of inflammatory foci, Fig. 7*I*, $P < 0.001$; % area of galectin-3, Fig. 7*N*, $P < 0.001$) and fibrosis (% area of sinusoidal fibrosis, Fig. 7*K*, $P < 0.001$; % area of PSR, Fig. 7*L*, $P < 0.001$) compared with vehicle while % area of α-SMA and Col1a1 were unaffected (Fig. 7, *O* and *P*, $P > 0.05$). The total content of individual quantitative histological markers is shown in Supplemental Fig. S5*D*.

Differential Effects of Pharmacological and Dietary Intervention on Hepatic Transcriptome Signatures in CDAA-HFD Mice

Hepatic transcriptome signatures were profiled in CDAA-HFD mice following semaglutide or lanifibranor treatment intervention or dietary intervention (Supplemental Fig. S6). A PCA plot of the 500 most variable genes demonstrated a clear group-wise according to treatment intervention, indicating highly stable and reproducible liver transcriptome signatures in the individual study groups (Supplemental Fig. S6*A*). Treatment interventions had different effects on the liver transcriptome in CDAA-HFD mice, as reflected by the total number of DEGs compared with vehicle (Supplemental Fig. S6*B*; chow, 11,043; chow reversal, 9,860; lanifibranor, 6,737; semaglutide, 6,392). A total of 2,066 DEGs were shared between all four groups (Supplemental Fig. S6*C*). Chow reversal was the treatment intervention paradigm that promoted a transcriptional profile most resembling that of the chow control group (Supplemental Fig. S6*A*). For chow reversal and lanifibranor interventions, transcriptional changes included a wide-spread upregulation of genes related to cholesterol biosynthesis and glucose and lipid metabolism and a general downregulation of genes related to hepatocellular cell death, inflammation, and ECM organization. Semaglutide showed only discrete effects on candidate markers of MASH and fibrosis (Supplemental Fig. S6*D*).

DISCUSSION

The current study profiled liver disease progression and clinically relevant treatment interventions in the CDAA-HFD mouse model of MASH and fibrosis. CDAA-HFD mice demonstrate rapid disease progression with early development of manifest MASH and mild/moderate fibrosis. Late-stage liver disease in CDAA-HFD mice was characterized by advanced fibrosis and tumor development. Lanifibranor, but not semaglutide, reversed MASH after preventive and treatment intervention in CDAA-HFD mice. In contrast, both lanifibranor and semaglutide improved a wide range of fibrosis markers in response to preventative intervention. The differential outcomes of preventative and treatment intervention in CDAA-HFD mice highlight the importance of timing treatment initiation for detecting antifibrotic drug effects in the model. Because of the lack of a clinical translational obese dysmetabolic phenotype, the model shows limitations in preclinical drug discovery as it is most applicable to profile directly liver-targeted drug candidates. Collectively, our findings further support the utility of the CDAA-HFD mouse model in preclinical drug development.

Liver biopsy endpoints in clinical trials for MASH are currently based on semiquantitative histopathological scoring systems (36) among which the MASH Clinical Research Network (CRN) is the most widely used system. As for all histopathological scoring systems, the MASH CRN system is inherently limited by inter- and intraobserver variability, which also extends to preclinical studies using clinically derived scoring variables (37). We have recently developed and implemented an AI pipeline, termed GHOST, enabling automated and unbiased histopathological scoring of NAS and fibrosis stage in the Gubra-Amylin NASH (GAN) diet-induced obese (DIO) mouse model of MASH. In the current study, GHOST was adapted and validated for use in the CDAA-HFD model. Considering the high degree of concordance between manual and GHOST-based histopathological scoring, the GHOST platform was applied to all CDAA-HFD mouse experiments in the present study.

We report that CDAA-HFD feeding accelerated disease progression with hepatic steatosis and lobular inflammation reaching maximal severity within only 3 wk. Importantly, fibrosis was detected in all animals after 6 wk of CDAA-HFD feeding with highly consistent progression to advanced fibrosis (*stage F3*, bridging fibrosis) after 12 wk of dieting. Overall, the CDAA-HFD mouse model consistently develops histological hallmarks of progressive MASH and fibrosis, being in line with previous reports (11, 16). Liver fibrosis in CDAA-HFD

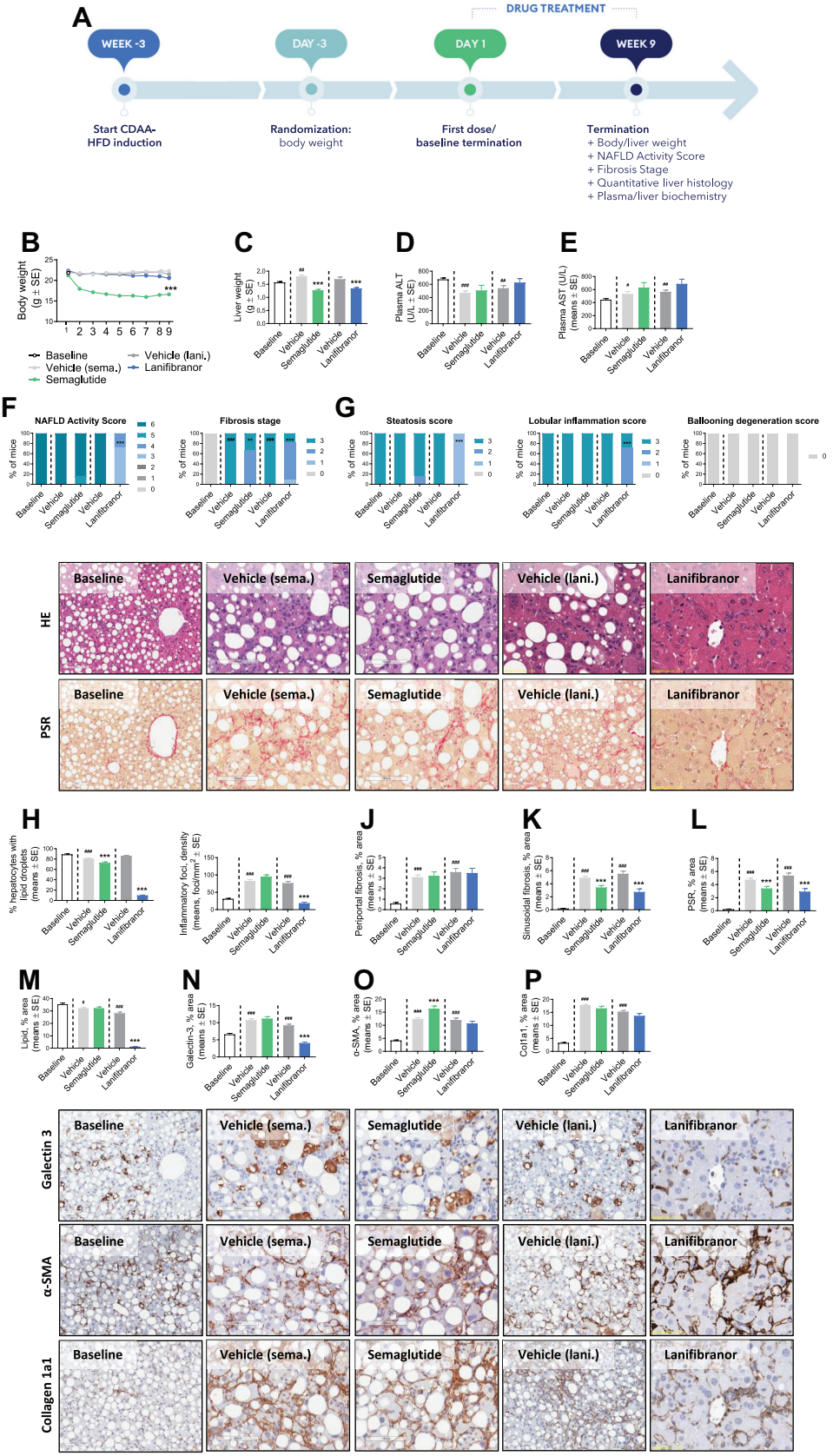

Figure 7. Preventive intervention with semaglutide and lanifibranor improves hallmarks of MASH and fibrosis. Mice were fed the CDAA-HFD diet for 3 wk ($n = 10$–12 per group) whereafter drug treatment commenced and was maintained for 9 wk. The baseline group was terminated on *study day 1*. *A*: study outline. *B*: body weight profile over the treatment period. *C*: liver weight. *D*: plasma ALT. *E*: plasma AST. *F*: NAFLD Activity Score (NAS) and fibrosis stage. *G*: steatosis, lobular inflammation, and ballooning degeneration scores. *H*–*P*: GHOST-based histomorphometrics on histopathological scoring variables of lipid-laden hepatocytes (*H*), inflammatory foci (*I*), and periportal/sinusoidal fibrosis (*J* and *K*), % area of picrosirius red (PSR) (*L*), proportionate (%) area of lipids (*M*), % area of inflammation (galectin-3; *N*), % area of α-SMA (fibrogenesis marker; *O*), and % area of Col1a1 (*P*). See Supplemental Fig. S5 for total liver histological marker levels. *Middle*: hematoxylin-eosin (HE) and PSR staining illustrating the development of steatosis and fibrosis in CDAA-HFD mice (scale bar, 100 µm). *Bottom*: representative photomicrographs of galectin-3, α-SMA, and Col1a1 immunostainings (scale bar, 100 µm). $*P < 0.05$, $**P < 0.01$, $***P < 0.001$ vs. corresponding vehicle and $\#P < 0.05$, $\#\#P < 0.01$, $\#\#\#P < 0.001$ vs. Baseline (Dunnett's test one-factor linear model). α-SMA; α-smooth muscle action; ALT, alanine aminotransferase; AST, aspartate aminotransferase; CDAA-HFD, choline-deficient L-amino acid defined-high-fat diet; GHOST, Gubra Histopathological Objective Scoring Technology; MASH, metabolic dysfunction-associated steatohepatitis; NAFLD, nonalcoholic fatty liver disease.

mice did not progress to manifest cirrhosis (*stage F4*), supporting that further extended CDAA-HFD feeding regimens are required to induce cirrhosis in the model (16). In contrast, rats have been reported to develop cirrhosis after 14 wk of CDAA-HFD dieting, indicating species differences in the sensitivity to CDAA and high-fat dieting (15, 38). Progressive changes in histopathological scores were paralleled by robust increases in quantitative histological markers of steatosis, inflammation, and fibrosis over the course of liver disease progression in CDAA-HFD mice. In contrast to incremental increases in quantitative inflammation markers, histological markers of steatosis peaked after 6 wk of CDAA-HFD and declined thereafter. This could suggest a precirrhotic state in CDAA-HFD mice, as spontaneous regression of steatosis is often observed in patients with MASH before the onset of cirrhosis, which, in some cases, can result in a complete loss of liver fat ("burn-out MASH") when cirrhosis has become manifest (39). Considering that steatosis scores remained maximal throughout the longitudinal study in CDAA-HFD mice, this emphasizes the advantage of complementing histopathological scores by quantitative histology to detect changes in histological hallmarks of MASH. In contrast to patients with MASH (40), CDAA-HFD feeding did not induce ballooning degeneration. Hepatocyte ballooning has also been reported as marginal or absent in other rodent models of MASH, making composite NAS in these species largely determined by the grade of hepatic steatosis and inflammation (24, 41). However, some studies have reported mild ballooning in CDAA-HFD mice (13, 42, 43), possibly explained by differences in histopathological assessments. For example, there is not a complete overlap in hepatocyte ballooning morphology between humans and rodents, as rodent models of MASH exhibit more prominent microvesicular fat accumulation making it challenging to distinguish from ballooning degeneration (44).

In addition to the fast onset and progression of MASH and fibrosis, CDAA-HFD mice developed macroscopic liver tumors after 20 wk of dieting. This is consistent with previously reported studies in the model, which further show the presence of oncofetal markers *Afp* and *Gpc3* and HCC-markers glypican-3 and/or glutamine synthetase, supporting the notion of human-like HCC (13, 16). Interestingly, we find tumor formation preceded by the acquisition of a pro-tumorigenic gene expression signature, with the regulation of several molecular markers of human HCC, being manifest after 3 wk of diet induction. This suggests a highly pro-metastatic microenvironment in the model. Overall, the CDAA-HFD model represents an accelerated diet-induced model of liver tumor formation, also making it a useful model for studying MASH-associated tumorigenesis without the use of genetic modifications or hepatotoxins (13, 16).

Characterization of the clinical translatability of preclinical models of MASH is essential in guiding the selection of models in preclinical drug discovery. To this end, we applied the unbiased MHPS ranking system, recently applied to score the translatability of commonly used preclinical MASLD models (34), to assess the proximity of the current CDAA-HFD model to human MASH. To define the clinical translatability, the MHPS ranking system evaluates metabolic phenotype, liver histology, and liver transcriptomics (benchmarked against human MASH), providing separate scores for metabolic relevance and ability to induce MASH-fibrosis (34). As liver pathology in the CDAA-HFD model is driven by direct liver lipotoxicity fueled by the deficient hepatic fatty acid oxidation and triglycerides export (8, 9), the model does not present the metabolic hallmarks of human MASH. The model is nonobese, displays loss of lean tissue mass and does not feature glucose intolerance and insulin resistance. Also, the CDAA-HFD model is characterized by hypophagia, hypercatabolism with a proportional loss of liver mass, which, however, is counteracted in excess by the lipotropic effect of dietary choline deficiency (41, 45). This limitation is reflected in a low ranking in the metabolic-related arm of the MHPS, in line with other rodent models based on CDAA-HFD feeding regiments, highlighting model divergence from the metabolic profile characteristic of human MASH. Conversely, models based on Western Diets, such as GAN, which are high in fat, refined carbohydrates (especially fructose), and cholesterol better reflect the natural history of the disease, affording closer metabolic resemblance to human MASH disease, but at the cost of longer diet induction periods ($\geq$28 wk). The CDAA-HFD model demonstrates a higher score in the MASH-fibrosis arm of the MHPS ranking, reflecting the consistent progression of histological hallmarks of progressive MASH and fibrosis. Although the current CDAA-HFD mouse model scored slightly lower in the final MHPS MASH-fibrosis ranking compared with other CDAA-based models (due to the absence of ballooning degeneration and end-stage cirrhosis), it outranked these models in terms of fibrosis severity (*stage F3*) and afforded better transcriptional resemblance (DHPS layer) reflecting molecular events related to human MASH-fibrosis. The differential ranking in the MASH-metabolic versus MASH-fibrosis arm of the MHPS ranking system further supports the notion, that no single mouse model recapitulates the entire spectrum of pathological features characteristic to human MASH. The current CDAA-HFD model presents a valuable liver-specific model for studying drugs targeting the liver as it is not confounded by extrahepatic metabolic effects, but is not recommended for evaluating disease etiology and drugs targeting general metabolic features of MASH.

To evaluate the reversibility of CDAA-HFD diet-induced hepatic fibrosis, we assessed the effect of dietary intervention, i.e., shifting to chow feeding after 6 wk of CDAA-HFD induction (chow reversal). Dietary intervention for 8 wk resulted in recovery of CDAA-HFD induced weight loss, hepatomegaly as well as complete resolution of steatosis and marked improvement of inflammation. Consistent with previous reports (13), dietary intervention improved fibrosis stage and quantitative histological markers of fibrosis in CDAA-HFD mice, albeit to a moderate degree, suggesting that dietary intervention was sufficient to halt de novo collagen formation but did not significantly stimulate clearance of existing fibers. The methionine-choline-deficient (MCD) diet-induced mouse model of MASH also shows partial regression of fibrosis upon dietary intervention (46). In contrast to the moderate therapeutic effect on fibrosis, dietary intervention markedly reduced α-SMA expression, a well-established marker of fibrogenesis (47), and suppressed multiple genes involved in ECM organization suggesting ongoing tissue remodeling, making it possible that prolonged dietary intervention ($\geq$8

wk) could further improve histological endpoints in the model.

The CDAA-HFD mouse model is commonly used in preclinical drug discovery (41, 48, 49), making it pertinent to rigorously pharmacologically validate the model. To this end, we evaluated the therapeutic efficacy of six compounds which have been profiled in phase-2/3 clinical trials for MASH, including semaglutide (long-acting GLP-1R agonist) (17), lanifibranor (PPAR-α/δ/γ agonist) (18), elafibranor (PPAR-α/δ agonist (19), OCA (FXR agonist) (20), firsocostat (ACC inhibitor) (21), and resmetirom (THR-β agonist) (5). All compounds were evaluated in the context of treatment intervention, i.e., initiation of treatment after the onset of fibrosis (6 wk of treatment, starting after 6 wk of CDAA-HFD feeding).

The six clinical-stage compounds demonstrated distinct efficacy profiles in CDAA-HFD mice. Whereas semaglutide markedly reduced body weight in CDAA-HFD mice, all other compounds tested were weight-neutral, being consistent with corresponding clinical trials (5, 17–21). Successful weight loss (≥5%–10%) is considered a contributing factor for improved liver-related outcomes in patients with MASH (50). The robust weight loss (≈25%) following semaglutide treatment in CDAA-HFD mice is within the range previously reported for corresponding studies in DIO-MASH mice (27). It should be emphasized that CDAA feeding induces a hypercatabolic (cachectic) state in rodents (41), and a further drop in body weight may therefore not be a desirable outcome in CDAA-HFD mice. Interestingly, interventional semaglutide therapy significantly reduced hepatomegaly while having no effects on quantitative liver histological endpoints in CDAA-HFD mice. Notably, improved hepatomegaly was not reflected in a lower fraction of liver fat or lipid-laden hepatocytes, making it unlikely that changes in liver lipid markers could explain the benefits of liver weight alone. As the CDAA-HFD mice demonstrated molecular and histological features of hepatic tumorigenesis, we cannot rule out that semaglutide may have antineoplastic effects in the CDAA-HFD mouse as recently demonstrated for DIO-MASH mice (41), which could potentially contribute to reducing liver mass. It is noteworthy that semaglutide also failed to improve NAS in the model, contrasting previous studies in DIO-MASH mice (25, 27, 51, 52) as well as a clinical phase-2 trial indicating significant benefits on liver histology, notably steatosis scores, in patients with MASH (17). Given the lack of GLP-1 receptor expression in the rodent and human liver (53, 54), the hepatoprotective effects of semaglutide could be an indirect consequence of reduced food intake and body weight, improved fat mass, and reduced insulin resistance. As CDAA-HFD mice demonstrated very low HOMA-IR, reflecting low plasma insulin levels, this would point toward a highly insulin-sensitive state, which could preclude the evaluation of drugs acting primarily by increasing insulin sensitivity. As a result, DIO-MASH mouse models may be more suitable for characterizing anti-MASH drug candidates with predominant extrahepatic mechanisms of action.

In contrast to CDAA-HFD mice, both lanifibranor and elafibranor have been reported to promote robust weight loss in DIO-MASH mouse models (27, 35, 52). It is noteworthy that our longitudinal phenotyping study in CDAA-HFD mice indicated progressively reduced hepatic PPAR-α mRNA expression while PPAR-δ and PPAR-γ mRNA levels were increased. These hepatic PPAR transcriptional dynamics have not been observed in DIO-MASH mice (27). Although a comparative organ map of PPAR expression in CDAA-HFD versus DIO-MASH mice remains to be reported, our study suggests that CDAA-HFD feeding may render mice less prone to the weight loss-promoting effects of PPAR agonists. PPAR-α agonists are well-known to promote weight loss in mice due to combined effects of appetite suppression and thermogenesis in rodents (55–58). These characteristic metabolic effects of PPAR-α agonists are not observed in humans, being attributed to markedly higher expression and different tissue distribution of PPAR-α in rodents (55–57). On average it is estimated that hepatocyte PPAR-α mRNA levels are 10–20 times higher in rodents compared with humans, which underlies the potent effects of PPAR-α agonists on hepatic metabolism that is accompanied by peroxisomal proliferation-induced liver hypertrophy in rodents, but not humans (59, 60). The rodent-specific liver hypertrophic effect of PPAR-α stimulation could therefore explain why lanifibranor and elafibranor did not reduce hepatomegaly while markedly improving NAS, driven by reduced steatosis and inflammation scores, and corresponding quantitative histological markers in CDAA-HFD mice. The histological outcomes of lanifibranor and elafibranor treatment on hallmarks of MASH are in line with previous studies in CDAA-HFD and DIO-MASH mice (25, 27, 43). Although only elafibranor improved fibrosis stage both compounds significantly reduced quantitative fibrosis histology in CDAA-HFD mice, implying that PPAR-γ activation is not obligatory for achieving anti-fibrotic effects of PPAR agonists in the model. Although the current study did not assess pharmacokinetics of the individual compounds profiled in CDAA-HFD mice, elafibranor has been reported to undergo extensive enterohepatic recycling, which may potentially enhance its liver-targeted effects (61). The improvement in liver steatosis is proposed to be predominantly mediated by PPAR-α (lanifibranor, elafibranor), whereas suppression of hepatic inflammation and macrophage activation is due to stimulated PPAR-δ (lanifibranor, elafibranor) and PPAR-γ (lanifibranor) activity (62, 63). The PPAR-γ component has also been demonstrated to be essential for lanifibranor-induced inhibition of hepatic stellate cell activation in vitro and may, at least in part, explain lanifibranor's antifibrotic effects in DIO-MASH mice (27, 43). It should be emphasized that outcomes of lanifibranor and elafibranor in CDAA-HFD mice are not entirely consistent with data reported from corresponding clinical trials in patients with MASH. In the NATIVE phase-2 trial, lanifibranor significantly increased the proportion of patients with MASH resolution and at least 1-stage improvement of fibrosis (18). In addition, elafibranor demonstrated no histological benefits in the RESOLVE-IT phase-3 trial (64) while significantly reducing NAS and fibrosis scores in patients with MASH (65) achieving the modified primary outcome (no fibrosis worsening) in the GOLDEN-505 phase-2 trial (19). Based on positive outcomes in the ELATIVE phase-3 trial (66), elafibranor recently received accelerated FDA approval for the treatment of the rare liver disease primary biliary cholangitis (PBC).

OCA demonstrated modest therapeutic efficacy in CDAA-HFD mice, as evidenced by only reducing lipid accumulation with no additional improvements in other metabolic and histological endpoints. This contrasts the benefits on steatosis, inflammation, and fibrosis histology reported in

DIO-MASH and *ob/ob*-MASH mouse models (25, 67–69). OCA improves liver health by modulation of immunoinflammatory and fibrogenic responses through regulation of cholesterol lipoprotein and bile acid metabolism (70). However, as the CDAA-HFD mouse is characterized by nutritional deficiency, defective VLDL-triglyceride export, and dysregulated bile acid homeostasis (11, 34, 65, 71), this may account for the limited hepatoprotective effects of OCA in the model. The lack of liver histological effects of OCA in CDAA-HFD mice is contrasting clinical data. In patients with MASH, OCA has been reported to significantly improve fibrosis scores, but not NAS, in the FLINT phase-2 trial (72), whereas the opposite effect has been reported in the pivotal REGENERATE trial (20). A recent follow-up study, using a more rigorous consensus panel analysis of liver biopsies from the REGENERATIVE trial, confirmed antifibrotic efficacy of OCA (73). As for elafibranor, OCA has been approved for the treatment of PBC (74).

Firsocostat effectively reduced hepatomegaly and steatosis but had no effect on inflammation and fibrosis endpoints in CDAA-HFD mice. Firsocostat is a selective inhibitor of ACC1/2, the rate-limiting enzyme in de novo lipogenesis, thereby decreasing hepatic lipid synthesis while increasing fatty acid oxidation to reduce hepatic lipid burden and lipotoxic stress (75). In contrast, 8 wk of firsocostat (GS-0976) treatment, starting after 4 wk of CDAA-HFD diet induction, has been reported to attenuate steatosis, inflammation, and fibrosis in CDAA-HFD mice (76), suggesting greater histological effects of firsocostat at more early stages of liver disease in CDAA-HFD mice. Firsocostat also improved NAS (driven by reductions in steatosis scores) and quantitative fibrosis histology in Western diet-fed melanocortin 4 receptor-deficient mice (77). Although the anti-steatotic efficacy of firsocostat in MASH mouse models is consistent with a 12-wk proof-of-concept trial using non invasive MRI-based assessment of liver fat content in patients with MASH (78), firsocostat had no significant effect on the primary histological end point ($\geq$1-stage improvement in fibrosis without worsening of MASH) in the subsequent 48-wk ATLAS phase-2 trial (21).

Resmetirom (Rezdiffra) is the first FDA-approved drug therapy for MASH, based on positive outcomes of the pivotal phase-3 MAESTRO-NASH trial demonstrating significant benefits on both NAS and fibrosis stage, albeit with a modest placebo-adjusted response rate and effect size (5). Resmetirom has been reported effective in reducing hepatic steatosis and metabolic biomarkers in DIO-MASH mice (79–81). Our study indicates that resmetirom exhibited very limited therapeutic effects in CDAA-HFD mice, as indicated by minor improvements in liver weight and the percentage of lipid-laden hepatocytes but with no further benefits on liver histology. Resmetirom is a liver-targeted THR-β agonist that improves dyslipidemia and steatosis by regulating lipid metabolism by stimulation of β-oxidation and free fatty acid uptake, as well as reducing VLDL production and secretion (82). As the CDAA-HFD disrupts normal lipid transport mechanisms, particularly VLDL packaging and secretion, this might render resmetirom ineffective in ameliorating the severe MASH phenotype in CDAA-HFD mice.

Implementation of dietary intervention (chow-reversal) served to determine the reversibility of CDAA-HFD induced MASH and fibrosis. The effectiveness of chow-reversal is underscored by the highly consistent, complete regression of steatosis with substantial improvements in liver inflammation and fibrosis markers in CDAA-HFD mice. This applied to both histopathological scores and corresponding quantitative histological outcomes, which exceeded that attained by any drug treatment intervention profiled in the current study. As such, chow-reversal may thus be instrumental as an interventional paradigm for benchmarking the effectiveness of novel drug candidates in the model.

To consider the impact of the timing of pharmacotherapy in the CDAA-HFD mouse model, semaglutide and lanifibranor were also profiled in the context of preventive therapy by initiating drug treatment before the onset of fibrosis. In this setting, preventive therapy was performed over 9 wk, starting after 3 wk of CDAA-HFD feeding. As for interventional treatment, preventive semaglutide therapy robustly reduced body weight (−25%) and liver weight. It is noteworthy that preventive semaglutide therapy also led to consistent improvements in the fibrosis stage, but not NAS, being corroborated by corresponding specific changes in quantitative fibrosis histology. The marginal or lack of effect on quantitative histological markers of steatosis and inflammation suggests that the antifibrotic effect was unrelated to liver lipid metabolism. Given that gene expression markers of fibrogenesis were largely unaffected by preventive semaglutide therapy, it is tempting to speculate that semaglutide stimulated collagen clearance rather than inhibiting de novo collagen synthesis. Considering that chow-reversal improved all biochemical, histological, and transcriptional hallmarks of MASH and fibrosis in the model, this renders it unlikely that semaglutide suppressed CDAA-HFD intake to reverse fibrosis. Accumulating evidence suggests that infiltration of immune cells into the liver plays an important role in the initiation and progression of fibrosis in MASH (83). In this regard, it has been speculated that GLP-1 receptor agonists may potentially inhibit infiltration and activation of GLP-1 receptor-expressing macrophages to ameliorate hepatic inflammation (84). In addition, gut barrier-protective mechanisms have been proposed to play a contributory role in the hepatoprotective effects of GLP-1 receptor agonists (85). In contrast to semaglutide, preventive lanifibranor therapy was weight-neutral in CDAA-HFD mice and led to marked improvements in MASH, as evidenced by a $\geq$2 point reduction in NAS attributed to reduced steatosis and lobular inflammation scores, which was emphasized by substantial improvements in corresponding quantitative histological markers. Preventive lanifibranor therapy also resulted in a consistent $\geq$1 point improvement in fibrosis stage concurrent with reduced %-area of PSR staining. Given the more pronounced efficacy of preventive lanifibranor therapy, as compared with more delayed treatment intervention, this emphasizes the importance of treatment timing to obtain maximal drug therapeutic efficacy in the model.

In conclusion, the CDAA-HFD mouse represents an accelerated model of MASH and fibrosis, which is applicable for probing the efficacy of novel drug candidates with liver-directed mode of action. The current study serves to guide the application of the CDAA-HFD mouse model in preclinical drug discovery, emphasizing the importance of treatment timing. One limitation of the model, however, is that

CDAA-HFD mice develop progressive MASH and fibrosis in the absence of metabolic hallmarks of MASH, such as obesity and (pre)diabetes, thus not being suitable for targeting extrahepatic metabolic drivers of MASH. Accordingly, compounds with predominantly intrahepatic or extrahepatic mode of action, respectively, will likely display differential efficacy in the CDAA-HFD mouse model. Future studies should therefore aim to determine efficacy profiles of novel drug candidates with different modes of action to further delineate the advantages and limitations of the model in preclinical drug development for MASH.

DATA AVAILABILITY

The RNA sequencing datasets generated in the current study are available in the Gene Expression Omnibus (GEO) repository; https://www.ncbi.nlm.nih.gov/geo/; accession number (GSE269493). Other data that support the findings of this study are available from the corresponding author upon reasonable request. Some data may not be made available because of privacy or ethical restrictions.

SUPPLEMENTAL MATERIAL

Supplemental Figs. S1–S6 and Table S1: https://doi.org/10.6084/m9.figshare.27003139.

DISCLOSURES

M.H.N., J.N.M., M.B.M., D.O., S.P., M.W.A., H.H.H., and M.F. are employed by Gubra. M.H.N., J.N.M., D.O., S.P., M.W.A., H.H.H., and M.F. are shareholders in Gubra. J.W.P. is an Eli Lilly and Company employee and may own company stock or possess stock options. L.M.H. and S.V. are employed by Novo Nordisk. None of the other authors has any conflicts of interest, financial or otherwise, to disclose.

AUTHOR CONTRIBUTIONS

M.H.N., H.H.H., and M.F. conceived and designed research; M.H.N. and J.N.M. performed experiments; M.H.N., J.N.M., M.B.M., S.E.P., M.W.A., I.K., E.P., L.M.H., and H.H.H. analyzed data; M.H.N., D.O., S.E.P., M.V., H.H.H., and M.F. interpreted results of experiments; M.H.N., J.N.M., M.B.M., D.O., S.E.P., M.W.A., I.K., and L.M.H. prepared figures; M.H.N. drafted manuscript; M.H.N., D.O., I.K., J.W.P., S.V., H.H.H., and M.F. edited and revised manuscript; M.H.N., J.N.M., M.B.M., D.O., S.E.P., M.W.A., I.K., E.P., M.V., L.M.H., J.W.P., S.V., H.H.H., and M.F. approved final version of manuscript.

REFERENCES

1. **Ekstedt M**, **Hagström H**, **Nasr P**, **Fredrikson M**, **Stål P**, **Kechagias S**, **Hultcrantz R.** Fibrosis stage is the strongest predictor for disease-specific mortality in NAFLD after up to 33 years of follow-up. *Hepatology* 61: 1547–1554, 2015. doi:10.1002/hep.27368.
2. **Riazi K**, **Azhari H**, **Charette JH**, **Underwood FE**, **King JA**, **Afshar EE**, **Swain MG**, **Congly SE**, **Kaplan GG**, **Shaheen AA.** The prevalence and incidence of NAFLD worldwide: a systematic review and meta-analysis. *Lancet Gastroenterol Hepatol* 7: 851–861, 2022. doi:10.1016/S2468-1253(22)00165-0.
3. **Younossi ZM**, **Henry L.** Epidemiology of non-alcoholic fatty liver disease and hepatocellular carcinoma. *JHEP Rep* 3: 100305, 2021. doi:10.1016/j.jhepr.2021.100305.
4. **Globe Newswire.** Madrigal Pharmaceuticals Announces FDA Approval of Rezdiffra (resmetirom) for the Treatment of Patients with Noncirrhotic Nonalcoholic Steatohepatitis (NASH) with Moderate to Advanced Liver Fibrosis (Online). Madrigal Pharmaceuticals, Inc. https://ir.madrigalpharma.com/news-releases/news-release-details/madrigal-pharmaceuticals-announces-fda-approval-rezdiffratm [19 Mar 2024].
5. **Harrison SA**, **Bedossa P**, **Guy CD**, **Schattenberg JM**, **Loomba R**, **Taub R**, **Labriola D**, **Moussa SE**, **Neff GW**, **Rinella ME**, **Anstee QM**, **Abdelmalek MF**, **Younossi Z**, **Baum SJ**, **Francque S**, **Charlton MR**, **Newsome PN**, **Lanthier N**, **Schiefke I**, **Mangia A**, **Pericàs JM**, **Patil R**, **Sanyal AJ**, **Noureddin M**, **Bansal MB**, **Alkhouri N**, **Castera L**, **Rudraraju M**, **Ratziu V**; **MAESTRO-NASH Investigators.** A phase 3, randomized, controlled trial of resmetirom in NASH with liver fibrosis. *N Engl J Med* 390: 497–509, 2024. doi:10.1056/nejmoa2309000.
6. **Albhaisi SAM**, **Sanyal AJ.** New drugs for NASH. *Liver Int* 41, Suppl 1: 112–118, 2021. doi:10.1111/liv.14844.
7. **Dufour JF**, **Anstee QM**, **Bugianesi E**, **Harrison S**, **Loomba R**, **Paradis V**, **Tilg H**, **Wong VW**, **Zelber-Sagi S.** Current therapies and new developments in NASH. *Gut* 71: 2123–2134, 2022. doi:10.1136/gutjnl-2021-326874.
8. **Kodama Y**, **Kisseleva T**, **Iwaisako K**, **Miura K**, **Taura K**, **De Minicis S**, **Osterreicher CH**, **Schnabl B**, **Seki E**, **Brenner DA.** c-Jun N-terminal kinase-1 from hematopoietic cells mediates progression from hepatic steatosis to steatohepatitis and fibrosis in mice. *Gastroenterology* 137: 1467–1477.e5, 2009. doi:10.1053/j.gastro.2009.06.045.
9. **Caballero F**, **Fernández A**, **Matías N**, **Martínez L**, **Fucho R**, **Elena M**, **Caballeria J**, **Morales A**, **Fernández-Checa JC**, **García-Ruiz C.** Specific contribution of methionine and choline in nutritional nonalcoholic steatohepatitis: impact on mitochondrial S-adenosyl-L-methionine and glutathione. *J Biol Chem* 285: 18528–18536, 2010. doi:10.1074/jbc.M109.099333.
10. **Nakae D**, **Yoshiji H**, **Maruyama H**, **Kinugasa T**, **Denda A**, **Konishi Y.** Production of both 8-hydroxydeoxyguanosine in liver DNA and γ-Glutamyltransferase-positive hepatocellular lesions in rats given a choline-deficient, l-amino acid-defined diet. *Jpn J Cancer Res* 81: 1081–1084, 1990. doi:10.1111/j.1349-7006.1990.tb02515.x.
11. **Matsumoto M**, **Hada N**, **Sakamaki Y**, **Uno A**, **Shiga T**, **Tanaka C**, **Ito T**, **Katsume A**, **Sudoh M.** An improved mouse model that rapidly develops fibrosis in non-alcoholic steatohepatitis. *Int J Exp Pathol* 94: 93–103, 2013. doi:10.1111/iep.12008.
12. **Nakae D**, **Yoshiji H**, **Mizumoto Y**, **Horiguchi K**, **Shiraiwa K**, **Tamura K**, **Denda A**, **Konishi Y.** High incidence of hepatocellular carcinomas induced by a choline deficient L-amino acid defined diet in rats. *Cancer Res* 52: 5042–5045, 1992
13. **Ikawa-Yoshida A**, **Matsuo S**, **Kato A**, **Ohmori Y**, **Higashida A**, **Kaneko E**, **Matsumoto M.** Hepatocellular carcinoma in a mouse model fed a choline-deficient, L-amino acid-defined, high-fat diet. *Int J Exp Pathol* 98: 221–233, 2017. doi:10.1111/iep.12240.
14. **Honda T**, **Ishigami M**, **Luo F**, **Lingyun M**, **Ishizu Y**, **Kuzuya T**, **Hayashi K**, **Nakano I**, **Ishikawa T**, **Feng GG**, **Katano Y**, **Kohama T**, **Kitaura Y**, **Shimomura Y**, **Goto H**, **Hirooka Y.** Branched-chain amino acids alleviate hepatic steatosis and liver injury in choline-deficient high-fat diet induced NASH mice. *Metabolism* 69: 177–187, 2017. doi:10.1016/j.metabol.2016.12.013.
15. **Tølbøl KS**, **Stierstorfer B**, **Rippmann JF**, **Veidal SS**, **Rigbolt KTG**, **Schönberger T**, **Gillum MP**, **Hansen HH**, **Vrang N**, **Jelsing J**, **Feigh M**, **Broermann A.** Disease progression and pharmacological intervention in a nutrient-deficient rat model of nonalcoholic steatohepatitis. *Dig Dis Sci* 64: 1238–1256, 2019. doi:10.1007/s10620-018-5395-7.
16. **Wei G**, **An P**, **Vaid KA**, **Nasser I**, **Huang P**, **Tan L**, **Zhao S**, **Schuppan D**, **Popov YV.** Comparison of murine steatohepatitis models identifies a dietary intervention with robust fibrosis, ductular reaction, and rapid progression to cirrhosis and cancer. *Am J Physiol Gastrointest Liver Physiol* 318: G174–G188, 2020. doi:10.1152/AJPGI.00041.2019.
17. **Newsome PN**, **Buchholtz K**, **Cusi K**, **Linder M**, **Okanoue T**, **Ratziu V**, **Sanyal AJ**, **Sejling AS**, **Harrison SA**; **NN9931-4296 Investigators.** A placebo-controlled trial of subcutaneous semaglutide in nonalcoholic steatohepatitis. *N Engl J Med* 384: 1113–1124, 2021. doi:10.1056/nejmoa2028395.
18. **Francque SM**, **Bedossa P**, **Ratziu V**, **Anstee QM**, **Bugianesi E**, **Sanyal AJ**, **Loomba R**, **Harrison SA**, **Balabanska R**, **Mateva L**, **Lanthier N**, **Alkhouri N**, **Moreno C**, **Schattenberg JM**, **Stefanova-Petrova D**, **Vonghia L**, **Rouzier R**, **Guillaume M**, **Hodge A**, **Romero-Gómez M**, **Huot-Marchand P**, **Baudin M**, **Richard MP**, **Abitbol JL**, **Broqua P**, **Junien JL**, **Abdelmalek MF**; **NATIVE Study Group.** A randomized, controlled trial of the pan-PPAR agonist lanifibranor in NASH. *N Engl J Med* 385: 1547–1558, 2021. doi:10.1056/nejmoa2036205.

19. **Ratziu V**, **Harrison SA**, **Francque S**, **Bedossa P**, **Lehert P**, **Serfaty L**, **Romero-Gomez M**, **Boursier J**, **Abdelmalek M**, **Caldwell S**, **Drenth J**, **Anstee QM**, **Hum D**, **Hanf R**, **Roudot A**, **Megnien S**, **Staels B**, **Sanyal A**; **GOLDEN-505 Investigator Study Group.** Elafibranor, an agonist of the peroxisome proliferator-activated receptor-α and -δ, induces resolution of nonalcoholic steatohepatitis without fibrosis worsening. *Gastroenterology* 150: 1147–1159.e5, 2016 [Erratum in *Gastroenterology* 152: 2084, 2017]. doi:10.1053/j.gastro.2016.01.038.
20. **Younossi ZM**, **Ratziu V**, **Loomba R**, **Rinella M**, **Anstee QM**, **Goodman Z**, **et al.** Obeticholic acid for the treatment of non-alcoholic steatohepatitis: interim analysis from a multicentre, randomised, placebo-controlled phase 3 trial. *Lancet* 394: 2184–2196, 2019. doi:10.1016/S0140-6736(19)33041-7.
21. **Loomba R**, **Noureddin M**, **Kowdley KV**, **Kohli A**, **Sheikh A**, **Neff G**, **Bhandari BR**, **Gunn N**, **Caldwell SH**, **Goodman Z**, **Wapinski I**, **Resnick M**, **Beck AH**, **Ding D**, **Jia C**, **Chuang JC**, **Huss RS**, **Chung C**, **Subramanian GM**, **Myers RP**, **Patel K**, **Borg BB**, **Ghalib R**, **Kabler H**, **Poulos J**, **Younes Z**, **Elkhashab M**, **Hassanein T**, **Iyer R**, **Ruane P**, **Shiffman ML**, **Strasser S**, **Wong VW**, **Alkhouri N**; **ATLAS Investigators.** Combination therapies including cilofexor and firsocostat for bridging fibrosis and cirrhosis attributable to NASH. *Hepatology* 73: 625–643, 2021. doi:10.1002/HEP.31622.
22. **Kristiansen MN**, **Veidal SS**, **Rigbolt KT**, **Tølbøl KS**, **Roth JD**, **Jelsing J**, **Vrang N**, **Feigh M.** Obese diet-induced mouse models of nonalcoholic steatohepatitis-tracking disease by liver biopsy. *World J Hepatol* 8: 673–684, 2016. doi:10.4254/wjh.v8.i16.673.
23. **Matthews DR**, **Hosker JP**, **Rudenski AS**, **Naylor BA**, **Treacher DF**, **Turner RC.** Homeostasis model assessment: insulin resistance and β-cell function from fasting plasma glucose and insulin concentrations in man. *Diabetologia* 28: 412–419, 1985. doi:10.1007/BF00280883.
24. **Hansen HH**, **Ægidius HM**, **Oró D**, **Evers SS**, **Heebøll S**, **Eriksen PL**, **Thomsen KL**, **Bengtsson A**, **Veidal SS**, **Feigh M**, **Suppli MP**, **Knop FK**, **Grønbæk H**, **Miranda D**, **Trevaskis JL**, **Vrang N**, **Jelsing J**, **Rigbolt KTG.** Human translatability of the GAN diet-induced obese mouse model of non-alcoholic steatohepatitis. *BMC Gastroenterol* 20: 210–212, 2020. doi:10.1186/s12876-020-01356-2.
25. **Tølbøl KS**, **Kristiansen MN**, **Hansen HH**, **Veidal SS**, **Rigbolt KT**, **Gillum MP**, **Jelsing J**, **Vrang N**, **Feigh M.** Metabolic and hepatic effects of liraglutide, obeticholic acid and elafibranor in diet-induced obese mouse models of biopsy-confirmed nonalcoholic steatohepatitis. *World J Gastroenterol* 24: 179–194, 2018. doi:10.3748/wjg.v24.i2.179.
26. **Kleiner DE**, **Brunt EM**, **Van Natta M**, **Behling C**, **Contos MJ**, **Cummings OW**, **Ferrell LD**, **Liu YC**, **Torbenson MS**, **Unalp-Arida A**, **Yeh M**, **McCullough AJ**, **Sanyal AJ**; **Nonalcoholic Steatohepatitis Clinical Research Network.** Design and validation of a histological scoring system for nonalcoholic fatty liver disease. *Hepatology* 41: 1313–1321, 2005. doi:10.1002/hep.20701.
27. **Møllerhøj MB**, **Veidal SS**, **Thrane KT**, **Oró D**, **Overgaard A**, **Salinas CG**, **Madsen MR**, **Pfisterer L**, **Vyberg M**, **Simon E**, **Broermann A**, **Vrang N**, **Jelsing J**, **Feigh M**, **Hansen HH.** Hepatoprotective effects of semaglutide, lanifibranor and dietary intervention in the GAN diet-induced obese and biopsy-confirmed mouse model of NASH. *Clin Transl Sci* 15: 1167–1186, 2022. doi:10.1111/cts.13235.
28. **Dobin A**, **Davis CA**, **Schlesinger F**, **Drenkow J**, **Zaleski C**, **Jha S**, **Batut P**, **Chaisson M**, **Gingeras TR.** STAR: ultrafast universal RNA-seq aligner. *Bioinformatics* 29: 15–21, 2013. doi:10.1093/bioinformatics/bts635.
29. **Team RC.** R: A Language and Environment for Statistical Computing. Vienna, Austria: R Foundation for Statistical Computing, 2019. https://www.R-project.org/.
30. **Bailey MH**, **Tokheim C**, **Porta-Pardo E**, **Sengupta S**, **Bertrand D**, **Weerasinghe A**, **et al.** Comprehensive characterization of cancer driver genes and mutations. *Cell* 173: 371–385.e18, 2018 [Erratum in *Cell* 174: 1034–1035, 2018]. doi:10.1016/j.cell.2018.02.060.
31. **Bidkhori G**, **Benfeitas R**, **Klevstig M**, **Zhang C**, **Nielsen J**, **Uhlen M**, **Boren J**, **Mardinoglu A.** Metabolic network-based stratification of hepatocellular carcinoma reveals three distinct tumor subtypes. *Proc Natl Acad Sci USA* 115: E11874–E11883, 2018. doi:10.1073/pnas.1807305115.
32. **Ho CM**, **Lin KT**, **Shen R**, **Gu DL**, **Lee SS**, **Su WH**, **Jou YS.** Prognostic comparative genes predict targets for sorafenib combination therapies in hepatocellular carcinoma. *Comput Struct Biotechnol J* 20: 1752–1763, 2022. doi:10.1016/j.csbj.2022.04.008.
33. **Zender L**, **Villanueva A**, **Tovar V**, **Sia D**, **Chiang DY**, **Llovet JM.** Cancer gene discovery in hepatocellular carcinoma. *J Hepatol* 52: 921–929, 2010. doi:10.1016/j.jhep.2009.12.034.
34. **Vacca M**, **Kamzolas I**, **Harder LM**, **Oakley F**, **Trautwein C**, **Hatting M**, **et al.** An unbiased ranking of murine dietary models based on their proximity to human metabolic dysfunction–associated steatotic liver disease (MASLD). *Nat Metab* 6: 1178–1196, 2024. doi:10.1038/s42255-024-01043-6.
35. **Hansen HH**, **Pors S**, **Andersen MW**, **Vyberg M**, **Nøhr-Meldgaard J**, **Nielsen MH**, **Oró D**, **Madsen MR**, **Lewinska M**, **Møllerhøj MB**, **Madsen AN**, **Feigh M.** Semaglutide reduces tumor burden in the GAN diet-induced obese and biopsy-confirmed mouse model of NASH-HCC with advanced fibrosis. *Sci Rep* 13: 23056, 2023. doi:10.1038/s41598-023-50328-5.
36. **Ratziu V.** A critical review of endpoints for non-cirrhotic NASH therapeutic trials. *J Hepatol* 68: 353–361, 2018. doi:10.1016/j.jhep.2017.12.001.
37. **Davison BA**, **Harrison SA**, **Cotter G**, **Alkhouri N**, **Sanyal A**, **Edwards C**, **Colca JR**, **Iwashita J**, **Koch GG**, **Dittrich HC.** Suboptimal reliability of liver biopsy evaluation has implications for randomized clinical trials. *J Hepatol* 73: 1322–1332, 2020. doi:10.1016/j.jhep.2020.06.025.
38. **Karimkhanloo H**, **Keenan SN**, **Bayliss J**, **De Nardo W**, **Miotto PM**, **Devereux CJ**, **Nie S**, **Williamson NA**, **Ryan A**, **Watt MJ**, **Montgomery MK.** Mouse strain-dependent variation in metabolic associated fatty liver disease (MAFLD): a comprehensive resource tool for pre-clinical studies. *Sci Rep* 13: 4711, 2023. doi:10.1038/s41598-023-32037-1.
39. **Yeh MM**, **Brunt EM.** Pathology of nonalcoholic fatty liver disease. *Am J Clin Pathol* 128: 837–847, 2007. doi:10.1309/RTPM1PY6YGBL2G2R.
40. **Loomba R**, **Friedman SL**, **Shulman GI.** Mechanisms and disease consequences of nonalcoholic fatty liver disease. *Cell* 184: 2537–2564, 2021. doi:10.1016/j.cell.2021.04.015.
41. **Hansen HH**, **Feigh M**, **Veidal SS**, **Rigbolt KT**, **Vrang N**, **Fosgerau K.** Mouse models of nonalcoholic steatohepatitis in preclinical drug development. *Drug Discov Today* 22: 1707–1718, 2017. doi:10.1016/j.drudis.2017.06.007.
42. **Hoffmann C**, **Djerir NEH**, **Danckaert A**, **Fernandes J**, **Roux P**, **Charrueau C**, **Lachagès AM**, **Charlotte F**, **Brocheriou I**, **Clément K**, **Aron-Wisnewsky J**, **Foufelle F**, **Ratziu V**, **Hainque B**, **Bonnefont-Rousselot D**, **Bigey P**, **Escriou V.** Hepatic stellate cell hypertrophy is associated with metabolic liver fibrosis. *Sci Rep* 10: 3850, 2020. doi:10.1038/s41598-020-60615-0.
43. **Lefere S**, **Puengel T**, **Hundertmark J**, **Penners C**, **Frank AK**, **Guillot A**, **de Muynck K**, **Heymann F**, **Adarbes V**, **Defrêne E**, **Estivalet C**, **Geerts A**, **Devisscher L**, **Wettstein G**, **Tacke F.** Differential effects of selective- and pan-PPAR agonists on experimental steatohepatitis and hepatic macrophages ☆. *J Hepatol* 73: 757–770, 2020. doi:10.1016/j.jhep.2020.04.025.
44. **Farrell G**, **Schattenberg JM**, **Leclercq I**, **Yeh MM**, **Goldin R**, **Teoh N**, **Schuppan D.** Mouse models of nonalcoholic steatohepatitis: toward optimization of their relevance to human nonalcoholic steatohepatitis. *Hepatology* 69: 2241–2257, 2019. doi:10.1002/hep.30333.
45. **Suzuki-Kemuriyama N**, **Abe A**, **Nakane S**, **Uno K**, **Ogawa S**, **Watanabe A**, **Sano R**, **Yuki M**, **Miyajima K**, **Nakae D.** Nonobese mice with nonalcoholic steatohepatitis fed on a choline-deficient, L-amino acid-defined, high-fat diet exhibit alterations in signaling pathways. *FEBS Open Bio* 11: 2950–2965, 2021. doi:10.1002/2211-5463.13272.
46. **Itagaki H**, **Shimizu K**, **Morikawa S**, **Ogawa K**, **Ezaki T.** Morphological and functional characterization of non-alcoholic fatty liver disease induced by a methionine-choline-deficient diet in C57BL/6 mice. *Int J Clin Exp Pathol* 6: 2683–2696, 2013.
47. **Tsuchida T**, **Friedman SL.** Mechanisms of hepatic stellate cell activation. *Nat Rev Gastroenterol Hepatol* 14: 397–411, 2017. doi:10.1038/nrgastro.2017.38.
48. **Gallage S**, **Avila JEB**, **Ramadori P**, **Focaccia E**, **Rahbari M**, **Ali A**, **Malek NP**, **Anstee QM**, **Heikenwalder M.** A researcher's guide to preclinical mouse NASH models. *Nat Metab* 4: 1632–1649, 2022. doi:10.1038/s42255-022-00700-y.
49. **Hansen HH**, **Hansen G**, **Secher T**, **Feigh M**, **Veidal SS**, **Fosgerau K**, **Jelsing J**, **Vrang N.** Animal models of type 2 diabetes, obesity and nonalcoholic steatohepatitis – clinical translatability and applicability in preclinical drug development. In: *Translational Research Methods in Diabetes, Obesity, and Nonalcoholic Fatty Liver Disease*, edited by Krentz A, Weyer C, Hompesch M. Cham, Switzerland: Springer, 2019, p 369–403. doi:10.1007/978-3-030-11748-1_14.

50. **Patel NS**, **Doycheva I**, **Peterson MR**, **Hooker J**, **Kisselva T**, **Schnabl B**, **Seki E**, **Sirlin CB**, **Loomba R.** Effect of weight loss on magnetic resonance imaging estimation of liver fat and volume in patients with nonalcoholic steatohepatitis. *Clin Gastroenterol Hepatol* 13: 561–568.e1, 2015. doi:10.1016/j.cgh.2014.08.039.
51. **Nestor JJ**, **Parkes D**, **Feigh M**, **Suschak JJ**, **Harris MS.** Effects of ALT-801, a GLP-1 and glucagon receptor dual agonist, in a translational mouse model of non-alcoholic steatohepatitis. *Sci Rep* 12: 6666, 2022. doi:10.1038/S41598-022-10577-2.
52. **Monfeuga T**, **Norlin J**, **Bugge A**, **Gaalsgaard ED**, **Prada-Medina CA**, **Latta M**, **Veidal SS**, **Petersen PS**, **Feigh M**, **Holst D.** Evaluation of long acting GLP1R/GCGR agonist in a DIO and biopsy-confirmed mouse model of NASH suggest a beneficial role of GLP-1/glucagon agonism in NASH patients. *Mol Metab* 79: 101850, 2024. doi:10.1016/J.MOLMET.2023.101850.
53. **Pyke C**, **Heller RS**, **Kirk RK**, **Ørskov C**, **Reedtz-Runge S**, **Kaastrup P**, **Hvelplund A**, **Bardram L**, **Calatayud D**, **Knudsen LB.** GLP-1 receptor localization in monkey and human tissue: novel distribution revealed with extensively validated monoclonal antibody. *Endocrinology* 155: 1280–1290, 2014. doi:10.1210/en.2013-1934.
54. **Panjwani N**, **Mulvihill EE**, **Longuet C**, **Yusta B**, **Campbell JE**, **Brown TJ**, **Streutker C**, **Holland D**, **Cao X**, **Baggio LL**, **Drucker DJ.** GLP-1 receptor activation indirectly reduces hepatic lipid accumulation but does not attenuate development of atherosclerosis in diabetic male ApoE Mice (-/-). *Endocrinology* 154: 127–139, 2013. doi:10.1210/en.2012-1937.
55. **Gross B**, **Pawlak M**, **Lefebvre P**, **Staels B.** PPARs in obesity-induced T2DM, dyslipidaemia and NAFLD. *Nat Rev Endocrinol* 13: 36–49, 2017. doi:10.1038/NRENDO.2016.135.
56. **Harrington WW**, **Britt CS**, **Wilson JG**, **Milliken NO**, **Binz JG**, **Lobe DC**, **Oliver WR**, **Lewis MC**, **Ignar DM.** The Effect of PPARα, PPARδ, PPARγ, and PPARpan agonists on body weight, body mass, and serum lipid profiles in diet-induced obese AKR/J mice. *PPAR Res* 2007: 97125, 2007. doi:10.1155/2007/97125.
57. **Perreault M**, **Will S**, **Panza D**, **Gareski T**, **Harding K**, **Kubasiak D**, **Jalenak M**, **Gartrell K**, **Wang S**, **Bollag G**, **Artis DR**, **Ibrahim PN**, **Womack P**, **Lin JJ**, **Saiah E**, **Mansour TS**, **Vlasuk GP**, **Erbe DV**, **Tobin JF.** Modulation of nutrient sensing nuclear hormone receptors promotes weight loss through appetite suppression in mice. *Diabetes Obes Metab* 12: 234–245, 2010. doi:10.1111/J.1463-1326.2009.01157.X.
58. **Rachid TL**, **Penna-de-Carvalho A**, **Bringhenti I**, **Aguila MB**, **Mandarim-de-Lacerda CA**, **Souza-Mello V.** Fenofibrate (PPARα agonist) induces beige cell formation in subcutaneous white adipose tissue from diet-induced male obese mice. *Mol Cell Endocrinol* 402: 86–94, 2015 [Erratum in *Mol Cell Endocrinol* 413: 249, 2015]. doi:10.1016/J.MCE.2014.12.027.
59. **Holden PR**, **Tugwood JD.** Peroxisome proliferator-activated receptor alpha: role in rodent liver cancer and species differences. *J Mol Endocrinol* 22: 1–8, 1999. doi:10.1677/JME.0.0220001.
60. **Burri L**, **Thoresen GH**, **Berge RK.** The role of PPARα activation in liver and muscle. *PPAR Res* 2010: 542359, 2010. doi:10.1155/2010/542359.
61. **Cariou B**, **Hanf R**, **Lambert-Porcheron S**, **Zaïr Y**, **Sauvinet V**, **Noël B**, **Flet L**, **Vidal H**, **Staels B**, **Laville M.** Dual peroxisome proliferator-activated receptor α/δ agonist GFT505 improves hepatic and peripheral insulin sensitivity in abdominally obese subjects. *Diabetes Care* 36: 2923–2930, 2013. doi:10.2337/dc12-2012.
62. **Boubia B**, **Poupardin O**, **Barth M**, **Binet J**, **Peralba P**, **Mounier L**, **Jacquier E**, **Gauthier E**, **Lepais V**, **Chatar M**, **Ferry S**, **Thourigny A**, **Guillier F**, **Llacer J**, **Amaudrut J**, **Dodey P**, **Lacombe O**, **Masson P**, **Montalbetti C**, **Wettstein G**, **Luccarini JM**, **Legendre C**, **Junien JL**, **Broqua P.** Design, synthesis, and evaluation of a novel series of indole sulfonamide peroxisome proliferator activated receptor (PPAR) α/γ/δ triple activators: discovery of lanifibranor, a new antifibrotic clinical candidate. *J Med Chem* 61: 2246–2265, 2018. doi:10.1021/acs.jmedchem.7b01285.
63. **Staels B**, **Rubenstrunk A**, **Noel B**, **Rigou G**, **Delataille P**, **Millatt LJ**, **Baron M**, **Lucas A**, **Tailleux A**, **Hum DW**, **Ratziu V**, **Cariou B**, **Hanf R.** Hepatoprotective effects of the dual peroxisome proliferator-activated receptor alpha/delta agonist, GFT505, in rodent models of nonalcoholic fatty liver disease/nonalcoholic steatohepatitis. *Hepatology* 58: 1941–1952, 2013. doi:10.1002/hep.26461.
64. **Genfit press release.** GENFIT: Announces Results from Interim Analysis of RESOLVE-IT Phase 3 Trial of Elafibranor in Adults with NASH and Fibrosis (Online). https://ir.genfit.com/news-releases/news-release-details/genfit-announces-results-interim-analysis-resolve-it-phase-3.
65. **Rao A**, **van de Peppel IP**, **Gumber SJ**, **Karpen SJ**, **Dawson PA.** Attenuation of the hepatoprotective effects of ileal apical sodium dependent bile acid transporter (ASBT) inhibition in choline-deficient L-amino acid-defined (CDAA) diet-fed mice. *Front Med (Lausanne)* 7: 60, 2020. doi:10.3389/FMED.2020.00060.
66. **Kowdley KV**, **Bowlus CL**, **Levy C**, **Akarca US**, **Alvares-da-Silva MR**, **Andreone P**, **Arrese M**, **Corpechot C**, **Francque SM**, **Heneghan MA**, **Invernizzi P**, **Jones D**, **Kruger FC**, **Lawitz E**, **Mayo MJ**, **Shiffman ML**, **Swain MG**, **Valera JM**, **Vargas V**, **Vierling JM**, **Villamil A**, **Addy C**, **Dietrich J**, **Germain JM**, **Mazain S**, **Rafailovic D**, **Taddé B**, **Miller B**, **Shu J**, **Zein CO**, **Schattenberg JM**; **ELATIVE Study Investigators' Group.** Efficacy and safety of elafibranor in primary biliary cholangitis. *N Engl J Med* 390: 795–805, 2024. doi:10.1056/NEJMOA2306185.
67. **Goto T**, **Itoh M**, **Suganami T**, **Kanai S**, **Shirakawa I**, **Sakai T**, **Asakawa M**, **Yoneyama T**, **Kai T**, **Ogawa Y.** Obeticholic acid protects against hepatocyte death and liver fibrosis in a murine model of nonalcoholic steatohepatitis. *Sci Rep* 8: 8157, 2018. doi:10.1038/s41598-018-26383-8.
68. **Roth JD**, **Veidal SS**, **Fensholdt LKD**, **Rigbolt KTG**, **Papazyan R**, **Nielsen JC**, **Feigh M**, **Vrang N**, **Young M**, **Jelsing J**, **Adorini L**, **Hansen HH.** Combined obeticholic acid and elafibranor treatment promotes additive liver histological improvements in a diet-induced ob/ob mouse model of biopsy-confirmed NASH. *Sci Rep* 9: 9046, 2019. doi:10.1038/s41598-019-45178-z.
69. **Adorini L**, **Rigbolt K**, **Feigh M**, **Roth J**, **Erickson M.** Increased hepatoprotective effects of the novel farnesoid X receptor agonist INT-787 versus obeticholic acid in a mouse model of nonalcoholic steatohepatitis. *PLoS One* 19: e0300809, 2024. doi:10.1371/JOURNAL.PONE.0300809.
70. **Jhaveri MA**, **Kowdley KV.** New developments in the treatment of primary biliary cholangitis – Role of obeticholic acid. *Ther Clin Risk Manag* 13: 1053–1060, 2017. doi:10.2147/TCRM.S113052.
71. **Ipsen DH**, **Lykkesfeldt J**, **Tveden-Nyborg P.** Animal models of fibrosis in nonalcoholic steatohepatitis: do they reflect human disease? *Adv Nutr* 11: 1696–1711, 2020. doi:10.1093/ADVANCES/NMAA081.
72. **Neuschwander-Tetri BA**, **Loomba R**, **Sanyal AJ**, **Lavine JE**, **Van Natta ML**, **Abdelmalek MF**, **Chalasani N**, **Dasarathy S**, **Diehl AM**, **Hameed B**, **Kowdley KV**, **McCullough A**, **Terrault N**, **Clark JM**, **Tonascia J**, **Brunt EM**, **Kleiner DE**, **Doo E**; **NASH Clinical Research Network.** Farnesoid X nuclear receptor ligand obeticholic acid for non-cirrhotic, non-alcoholic steatohepatitis (FLINT): a multicentre, randomised, placebo-controlled trial. *Lancet* 385: 956–965, 2015 [Erratum in *Lancet* 385: 946, 2015 and in *Lancet* 387: 1618, 2016]. doi:10.1016/S0140-6736(14)61933-4.
73. **Sanyal AJ**, **Ratziu V**, **Loomba R**, **Anstee QM**, **Kowdley KV**, **Rinella ME**, **Sheikh MY**, **Trotter JF**, **Knapple W**, **Lawitz EJ**, **Abdelmalek MF**, **Newsome PN**, **Boursier J**, **Mathurin P**, **Dufour JF**, **Berrey MM**, **Shiff SJ**, **Sawhney S**, **Capozza T**, **Leyva R**, **Harrison SA**, **Younossi ZM.** Results from a new efficacy and safety analysis of the REGENERATE trial of obeticholic acid for treatment of pre-cirrhotic fibrosis due to non-alcoholic steatohepatitis. *J Hepatol* 79: 1110–1120, 2023. doi:10.1016/J.JHEP.2023.07.014.
74. **Nevens F**, **Andreone P**, **Mazzella G**, **Strasser SI**, **Bowlus C**, **Invernizzi P**, **Drenth JP**, **Pockros PJ**, **Regula J**, **Beuers U**, **Trauner M**, **Jones DE**, **Floreani A**, **Hohenester S**, **Luketic V**, **Shiffman M**, **van Erpecum KJ**, **Vargas V**, **Vincent C**, **Hirschfield GM**, **Shah H**, **Hansen B**, **Lindor KD**, **Marschall HU**, **Kowdley KV**, **Hooshmand-Rad R**, **Marmon T**, **Sheeron S**, **Pencek R**, **MacConell L**, **Pruzanski M**, **Shapiro D**; **POISE Study Group.** A placebo-controlled trial of obeticholic acid in primary biliary cholangitis. *N Engl J Med* 375: 631–643, 2016. doi:10.1056/NEJMOA1509840.
75. **Alkhouri N**, **Lawitz E**, **Noureddin M**, **DeFronzo R**, **Shulman GI.** GS-0976 (Firsocostat): an investigational liver-directed acetyl-CoA carboxylase (ACC) inhibitor for the treatment of non-alcoholic steatohepatitis (NASH). *Expert Opin Investig Drugs* 29: 135–141, 2020. doi:10.1080/13543784.2020.1668374.
76. **Lu Y**, **Su X**, **Zhao M**, **Zhang Q**, **Liu C**, **Lai Q**, **Wu S**, **Fang A**, **Yang J**, **Chen X**, **Yao Y.** Comparative RNA-sequencing profiled the differential gene expression of liver in response to acetyl-CoA carboxylase inhibitor GS-0976 in a mouse model of NASH. *PeerJ* 7: e8115, 2019. doi:10.7717/PEERJ.8115.

77. **Matsumoto M**, **Yashiro H**, **Ogino H**, **Aoyama K**, **Nambu T**, **Nakamura S**, **Nishida M**, **Wang X**, **Erion DM**, **Kaneko M.** Acetyl-CoA carboxylase 1 and 2 inhibition ameliorates steatosis and hepatic fibrosis in a MC4R knockout murine model of nonalcoholic steatohepatitis. *PLoS One* 15: e0228212, 2020. doi:10.1371/JOURNAL.PONE.0228212.
78. **Loomba R**, **Kayali Z**, **Noureddin M**, **Ruane P**, **Lawitz EJ**, **Bennett M**, **Wang L**, **Harting E**, **Tarrant JM**, **McColgan BJ**, **Chung C**, **Ray AS**, **Subramanian GM**, **Myers RP**, **Middleton MS**, **Lai M**, **Charlton M**, **Harrison SA.** GS-0976 reduces hepatic steatosis and fibrosis markers in patients with nonalcoholic fatty liver disease. *Gastroenterology* 155: 1463–1473.e6, 2018. doi:10.1053/J.GASTRO.2018.07.027.
79. **Kannt A**, **Wohlfart P**, **Madsen AN**, **Veidal SS**, **Feigh M**, **Schmoll D.** Activation of thyroid hormone receptor-β improved disease activity and metabolism independent of body weight in a mouse model of non-alcoholic steatohepatitis and fibrosis. *Br J Pharmacol* 178: 2412–2423, 2021. doi:10.1111/bph.15427.
80. **Zhang YH**, **Xie R**, **Dai CS**, **Gao HW**, **Zhou G**, **Qi TT**, **Wang WY**, **Wang H**, **Cui YM.** Thyroid hormone receptor-beta agonist HSK31679 alleviates MASLD by modulating gut microbial sphingolipids. *J Hepatol*. In press. doi:10.1016/j.jhep.2024.08.008.
81. **Wang X**, **Wang L**, **Geng L**, **Tanaka N**, **Ye B.** Resmetirom ameliorates NASH-model mice by suppressing STAT3 and NF-κB signaling pathways in an RGS5-dependent manner. *Int J Mol Sci* 24: 5843, 2023. doi:10.3390/IJMS24065843.
82. **Sinha RA**, **Bruinstroop E**, **Singh BK**, **Yen PM.** Nonalcoholic fatty liver disease and hypercholesterolemia: roles of thyroid hormones, metabolites, and agonists. *Thyroid* 29: 1173–1191, 2019. doi:10.1089/thy.2018.0664.
83. **Cai J**, **Zhang XJ**, **Li H.** The role of innate immune cells in nonalcoholic steatohepatitis. *Hepatology* 70: 1026–1037, 2019. doi:10.1002/hep.30506.
84. **Wang Y**, **Parlevliet ET**, **Geerling JJ**, **van der Tuin SJ**, **Zhang H**, **Bieghs V**, **Jawad AH**, **Shiri-Sverdlov R**, **Bot I**, **De Jager SC**, **Havekes LM**, **Romijn JA**, **Willems van Dijk K**, **Rensen PC.** Exendin-4 decreases liver inflammation and atherosclerosis development simultaneously by reducing macrophage infiltration. *Br J Pharmacol* 171: 723–734, 2014. doi:10.1111/bph.12490.
85. **Bang-Berthelsen CH**, **Holm TL**, **Pyke C**, **Simonsen L**, **Søkilde R**, **Pociot F**, **Heller RS**, **Folkersen L**, **Kvist PH**, **Jackerott M**, **Fleckner J**, **Vilién M**, **Knudsen LB**, **Heding A**, **Frederiksen KS.** GLP-1 induces barrier protective expression in Brunner's glands and regulates colonic inflammation. *Inflamm Bowel Dis* 22: 2078–2097, 2016. doi:10.1097/MIB.0000000000000847.